Study on Viscoplastic Constitutive Equation and Its Application to Some Engineering Problems

（和訳題目：粘塑性構成方程式とその応用に関する基礎的研究）

Doctor Thesis of
The University of Tokyo

Faculty of Engineering
Department of Nuclear Engineering

December 20, 1991.

Written by

Hirotoshi Hishida (97123)

（菱田博俊）

(1)

Study on Viscoplastic Constitutive Equation and Its Application to Some Engineering Problems

(和訳題目：粘塑性構成方程式とその応用に関する基礎的研究)

Doctor Thesis of
The University of Tokyo

Faculty of Engineering
Department of Nuclear Engineering

December 20, 1991.

Written by
Hirotoshi Hishida (97123)
(菱田博俊)

This paper is submitted as the thesis for a doctor's degree
to Department of Nuclear Engineering,
Faculty of Engineering,
The University of Tokyo
under the tutorship of Prof. Dr. G. Yagawa

The fourth publication on March 14, 12:00.

Key words

Chaboche's viscoplastic theory
Viscoplastic constitutive equation
First wall of a fusion reactor
Thermal fatigue
Neural network

(和訳：キーワード)

シャボーシュの粘塑性理論
粘塑性構成方程式
核融合炉第一壁
熱疲労
ニューラルネットワーク

Acknowledgments

The author expresses his greatest gratitude to Prof. Dr. G. Yagawa for his kind arrangement of the present studies. Acknowledgment is also expressed to Associate Prof. Dr. S. Yoshimura for his encouraging discussions and advices on the present studies.

The experiments and the identifications by a numerical program in the present studies could be carried out with hearty help of Prof. Dr. D. Munz of the Karlsruhe nuclear research center, Germany (Kernforschungszentrum Karlsruhe) to whom the author is greatly indebted. Furthermore, several members of the institute of Prof. Dr. D. Munz such as, Dr. B. Schinke, Mr. E. Diegele, Mr. J. Schwertel and Mr. K. Hornberg supported the research works providing theoretical works related with viscoplastic models, computational works related with parameter identification, programing and implementation of viscoplastic material model to FE-code ABAQUS, respectively. Sincere acknowledgment is expressed to them as well.

The studies on a neural network could be successfully carried out with advices and experiences of Dr. A. Yoshioka and Mr. T. Ohishi. The computational simulations with the Chaboche's parameters which were determined by a neural network could be carried out with kind help of Ms. M. Ohshima and Mr. Y. Kitajima. I would also like to thank them deeply.

With such members of the institute of Prof. Dr. G. Yagawa as Mr. P. Chang-Ryul, Mr. Y. Mochizuki, Ms. Z. Min-Yan, Mr. H. Kawai, Mr. K. Tohkai, Mr. R. Shioya and Mr. S. Hamada, I could have good discussions on the present studies. The secretaries, Ms. K. Chiba and Ms. K. Amemiya of the Tokyo University, and Mr. W. Klas and Ms. L. Borchardt of the Karlsruhe nuclear research center helped me in various official arrangements. Other members of the Karlsruhe nuclear research center, Dr. T. Fett, Mr. S. Rhe, Mr. W. Hartly, Mr. S. Karl, and the scientific assistants of the Tokyo University, Mr. M. Kurosawa, Mr. I. Hasegawa, Mr. H. Kawate, Mr. S. Itoh, Mr. A. Morita and Mr. J. Morikawa kindly provided me with excellent research environments. I would like to express my sincere thanks to all of them.

Contents

Table Index

Chapter 2 :

Chapter 3 :

Chapter 4 :

Chapter 5 :

Chapter 6 :

Appendices :

Figure Index

Chapter 2 :

Chapter 3 :

Chapter 4 :

Chapter 5 :

Chapter 6 :

Chapter 7 :

Chapter 8 :

Appendices :

Nomenclature

In this paper, the characters have been defined as follows :

σ_{ij} : stress

ε_{ij} : strain (total strain or true strain)

σ_{kk} : bulk stress

ε_{kk} : bulk strain

s_{ij} : deviatoric stress

e_{ij} : deviatoric strain

e^e_{ij} : elastic deviatoric strain

$e^p_{ij} = \varepsilon^p_{ij}$: inelastic deviatoric strain = inelastic strain

ε^e_{ij} : elastic strain

ε^t_{ij} : thermal strain

P : accumulated inelastic strain

J : elastic bulk modulus

G : elastic shear modulus

E : elastic modulus (Young's modulus)

n : Poisson's ratio

Y_{ij} : back stress (equilibrium or rest stress) = kinematic hardening modulus

R : stress component related with yield stress = isotropic hardening modulus

Z : over stress

K : drag stress

$R_0 = k$: inertial yield stress

n : a parameter related with over stress in Chaboche's constitutive equation

H and D : parameters related with back stress in Chaboche's constitutive equation

h and d : parameters related with yield stress in Chaboche's constitutive equation

r : hardening yield stress

T : temperature of the atmosphere

t : time

N : cycle number of a cyclic test or a fatigue test

O_{kp} : neural output value from the output unit k for input pattern p (the final output value)

V_{kj} : neural weight value between output unit k and hidden unit j

W_{ji} : neural weight value between hidden unit j and input unit i

H_{jp} : neural output value from hidden unit j for input pattern p

I_{ip} : neural output value from input unit i for input pattern p (the original input value)

g_k : neural off-set value of output unit k

h_j : neural off-set value of hidden unit j

T_{kp} : neural target value of output unit k for input pattern p

f : sigmoid activation function

In all cases, a tensor and a vector are noted with subscripts, and scalar is noted without a subscript. Time derivatives are always noted with an overmarked point.

In this paper, other functions except for the sigmoid activation function f are denoted by f_i or g_i.

While no special notation exists, the following state variables (s_{ij} - Y_{ij}) is normally called the effective stress, where s_{ij} may be replaced by σ_{ij}.

Other detailed notations are explained in the corresponding chapters.

1 Introduction

In the design of fusion reactors, the fractural safety of the structural components, especially of the first wall under the real operation conditions should be insured, because the first wall is directly in contact with plasma which is critical with respect to the lifetime for fusion reactor plants. Through cyclic operations, the first wall is exposed under thermal fatigue condition due to high heat flux irradiation and active cooling of water as well as temperature cycles, when the wall temperature exceeds around 400℃ (Ref. [1.1], [1.2]). In order to predict the lifetime of the first wall under this thermal fatigue condition, calculation of the stress-strain fields in the first wall has been done with linear thermo-elastic analyses (Ref. [1.3], [1.4]). The stress is, however, much larger than the yield stress of the materials, so that nonlinear thermo-inelastic analyses which is more available to describe the real phenomena would be necessary to address the fatigue behavior.

SS 316L SPH stainless steel is one of the best candidate materials for the first wall of a fusion reactor, because its properties are well known, it has excellent characteristics against creep conditions under high temperature surroundings and because it can be welded easily. In the present studies, type SS 316L SPH stainless steel is taken into consideration, which has considerable advantage against irradiation and high temperature conditions and which is candidated as the structural material of the future fusion reactors, for example, NET. The stainless steel shows some behavior like primary creep, called " cold creep " in the most interested temperature range for the first wall, from 25℃ to 400℃, which can not be explained by a plastic model. Furthermore, the stainless steel has over stress behavior under thermo-mechanical loading condition, while over stress is the stress which is correlated with inelastic strain rate. The inelastic strain rate is taken into consideration not in a plastic model but in a viscoplastic model. Therefore, a viscoplastic theory is expected to be considered in this present studies. Viscoplastic theories have been proposed by Walker, Chaboche, Miller and some other authors, in capability of describing many actual phenomena including modification of material behaviors under cyclic loading condition (Ref. [1.5]). Furthermore, J. Eftis showed that Chaboche's viscoplastic model appeared to be capable of modeling a wide range of inelastic material behaviors (Ref. [1.6], [1.7]). Therefore, Chaboche's viscoplastic theory is considered to be one of the best theories to describe the actual viscoplastic phenomena occurred on SS 316L SPH stainless steel material under the first wall conditions to predict its lifetime in the present research.

These viscoplastic constitutive equations have a number of material parameters, which should be determined based on the real material behaviors. However, no proper method to determine the suitable set of parameters (Ref. [1.8]) has been developed yet, since it is very difficult to refer various experimental data, for examples, cyclic curves, hardening curves, creep curves, relaxation curves and tensile curves, simultaneously to evaluate a set of parameters. Previously, each parameter was determined independently based on each material behaviors, while the physical significance of the obtained parameter set with respect to the entire material behaviors was not sufficiently insured. In the present studies, two approaches are proposed to evaluate the seven parameters included in the stationary temperature and uniaxial form of Chaboche's viscoplastic constitutive equations : the one is numerical curve fitting based on a least square method, and the other is neural parameter prediction. The both approaches can identify these parameters based on experimental material behaviors of uniaxial cyclic loading tests and succeeding relaxation tests

which show cyclic, hardening, tensile and relaxation behaviors. These two types of tests are easy to be carried out. Throughout these approaches, the most desirable means of determining these parameters so as to satisfy their physical significance in the viscoplastic behaviors referring to the experimental data are researched, which should result in the reliable prediction of the viscoplastic behavior of the first wall material.

The parameters included in Chaboche's constitutive equations are temperature dependent, and should modify the material behaviors under temperature variation. It is, however, difficult to determine these temperature-dependent parameters directly from experimental data under various temperature conditions. While Chaboche tried to find out his parameters under high temperature conditions, application of these parameters to thermal fatigue phenomena has not been reported (Ref. [1.9], [1.10], [1.11]). In the present studies, two sets of Chaboche's parameters are evaluated for two different temperature cases of T=200℃ and T=400℃. If the obtained parameters are applied for the lifetime prediction of the first wall, these two parameter sets are interpolated to be applicable to thermal fatigue condition as temperature-dependent parameters.

The objectives in the present studies are as follows :

1. To develop most appropriate methods to evaluate the parameters included in Chaboche's constitutive equations based on cyclic loading tests and succeeding relaxation tests with two type of approaches.

2. To apply Chaboche's theory with the obtained parameter sets to SS 316L SPH stainless steel and to discuss its characteristics with respect to the lifetime under the first wall conditions.

The present paper consists of nine chapters including the first chapter of introduction. The succeeding eight chapters are summarized as follows :

In Chapter 2, the backgrounds for the present studies are reviewed. At first, the typical thermo-mechanical problems on the first wall and the related current investigations are described. Some viscoplastic constitutive theories, which have already been proposed, are totally explained to clarify their characteristics.

In Chapter 3, Chaboche's theory is explained and discussed in connection with viscoplastic considerations on the first wall behaviors. The general form and the stationary temperature and uniaxial form of Chaboche's constitutive equations are listed with the physical meaning of each parameter included. Furthermore, theoretical simulations of various viscoplastic behaviors are shown.

In Chapter 4, experimental procedures to determine the parameters are introduced. Uniaxial cyclic loading tests and succeeding relaxation tests carried out on SS 316L SPH stainless steel test specimens under two different temperature conditions are reported. These experimental data are

necessary to determine the parameter set of Chaboche's uniaxial correlations correctly. The experimental method employed is new in a sense of the configuration of the test specimen chosen and the data recording system.

In Chapter 5, one approach, which is a numerical method to evaluate the parameters based on the least square method, is described in detail. Through the numerical procedures, the parameters are shown to be fitted to both experimental data of hysteresis loops and relaxation stress histories essentially based on the iterative means to approach the final parameter values corresponding to two different temperature cases of 200℃ and 400℃. The obtained set of parameters are confirmed as to the numerical (in the sense of data fitting) and physical suitability and fidelity with respect to their physical significances shown in the experimental data.

In Chapter 6, the other approach, which is a computational method with a neural network, is described in detail. Through the neural procedures, the parameters are predicted based on the experimental data. The procedures consist of three main parts, learning pattern production, network learning and prediction. During these procedures, it should be searched to find out the proper choice of input data, learning patterns so as to conserve the physical significances of the predicted parameter values. Through the prediction procedure, the output data of the neural computation as the parameter values can be obtained easily without any technical skill.

In Chapter 7, the fractural behavior of the first wall component under the typical thermal fatigue condition is calculated as an example by means of numerical analyses based on the finite element method using the Chaboche's parameter sets obtained by the numerical approach. The typical cyclic heat flux condition is employed without irradiation effects. Two dimensional thermal calculation and stress calculation are numerically carried out, where three kinds of stress strain fields evaluated based on bilinear, plastic and Chaboche's viscoplastic models are adopted and the results are compared with one another. From the results of these stress strain fields on the first wall, the lifetimes up to the crack initiation are calculated based on a fatigue law.

In Chapter 8, discussions are given on these two types of parameter evaluation approaches which have both advantages and disadvantages, and the best method based on the comparison of these studies is proposed. Chaboche's theory is also discussed in connection to its availability for the first wall behavior evaluation.

Finally in Chapter 9, all the studies are summarized and the conclusions obtained through the present studies are given. Some related studies are supplemented in the following appendices.

2 Related Backgrounds

2.1.1 Surroundings of the First Wall

The first wall, which faces plasma directly, is exposed under the serious surroundings due to huge heat loading, magnetic force and sputtering or erosion caused by normal operation, plasma disruption, eddy current and neutron irradiation (Ref. [2.1]). For a TOKAMAK (Ref. [2.2]) or a NET (the Next European Tours) type reactor (Ref. [2.3]), which has plasma enclosed in the magnetic field, the repeated heat loading under the normal pulse operation causes thermal fatigue conditions on the first wall, which is one of the dominant problems for the first wall design.

Based on the actual NET-design (Ref. [1.1], [2.4]) of the first wall, the first wall condition associated with thermal fatigue is as follows : The thermal condition on the first wall of a fusion reactor is caused by cooling effect due to coolant water and high heat flux of stationary operated neutron irradiation. On the outboard side (plasma side) surface, the surface heat flax $\dot{Q}$ is considered to be about 40 W/cm^2, which raises the temperature up to 400℃ (see point A shown in Figure 2.1.1.1). At the surface faced on the cooling water, the temperature is about 100℃ (see point B shown in Figure 2.1.1.1). Within the first wall, an internal heat generation $\dot{q}$ is considered to be about 11 W/cm^3 due to the neutron irradiation. As the results of this temperature difference, compressive stress and tensile stress are loaded on the outboard region and the water-surfaced region, respectively. The operation history of the above-mentioned typical reactor is shown in Figure 2.1.1.2. During the first 500 seconds (beam plus width), the temperature increases rapidly due to the plasma generated (start-up) and the stationary burn-on term continues. Then during the next 250 seconds, the temperature goes down rapidly and the stationary burn-off term continues. The magnitudes of the stress are estimated at points A and B, which are shown in Table 2.1.1.1, where σ^p and σ^e mean the stress calculated by inelastic and elastic material behavior, respectively. The total strain range $\Delta\varepsilon$ is around 0.3 to 0.5 % as shown in Figure 2.1.1.3.

Many types of fusion reactors are currently under preliminary design consideration, where the burn-on and -off cycle and the neutron flux are different from one other. Thermal conditions of some other typical reactors are shown in Table 2.1.1.2 (Ref. [1.2], [2.5], [2.6]). These are characterized with duty which is related to plant availability, start-up time which depends on wall material and its coolability, and wall loading which depends on plasma power.

2.1.2 Structural Failure Assessment for the First Wall

Because of the above mentioned conditions, thermal fatigue due to repeated heat flux, thermal shock due to plasma disruption, material corruption due to irradiation and magnetic force due to magnetic field are taken place on the first wall. In the present studies, the thermal fatigue is focused at. Through the fatigue, a comparatively large stress in the vicinity of the fatigue limit is repeatedly and slowly loaded on the wall material. It can be said that the life-time of a fusion reactor depends just on that of the first wall.

It is essentially complicated to predict the lifetime of the first wall under real operation condition with considering irradiation effect. Studies related with the failure assessment of the first wall with respect to each of the failure assessment, such as thermal fatigue simulation without considering irradiation effect (Ref. [2.7]), linear-thermal fatigue simulation with considering irradiation effect (Ref. [1.3], [1.4]), and development of irradiation apparatuses (Ref. [2.8]) have been done. Recently, the effect of irradiation to the lifetime and the thermal fatigue behaviors have gradually become to be revealed, while the stress has been calculated to be very large and some proposals for considering irradiation effect to the material behaviors have been done. It may be that a method to predict the lifetime based on non-linear numerical calculation should be employed as the next step. In this paper, non-linear numerical calculation with viscoplastic theory is applied to the lifetime prediction without considering the irradiation effect.

2.1.3 Candidate Material

The material characteristics data under the first wall condition are researched into for the wall design studies. No suitable metallic mono-material which stands against the huge heat loading, magnetic loading and sputtering or erosion due to irradiation has, however, been found yet, and the characteristics of the candidate material have not completely been revealed because experimental apparatuses were not appropriate enough for such studies. Since characteristics of stainless steel are well known in connection with design studies on a PWR (pressurized water reactor), a BWR (boiling water reactors) and a LMFBR (liquid metal fast breeder reactors), such stainless steel family of metallic material as SS 304 or SS 316 steel has thus generally been favored for a material of the first wall. It may be that the stainless steel will really be used for the structural material of the first wall in the future.

On the other hand, studies on other first wall materials have recently been started, for examples ceramics, low Z (atomic number of atom) material coated metals to prevent the lowering of temperature due to sputtering, and bimaterials such as metal welded with a heat resistive material or erosion resistive tungsten. These newly proposed material and bimaterial are expected to be resistive enough against the very severe first wall condition, which metallic material can not individually be qualified for. The behavior under the first wall condition of such materials as stated above, however, has not been understood clearly yet.

Therefore, the failure assessment on stainless steel, inevitably candidated as the material for the first wall components, becomes still very important. Through the present studies, SS 316L SPH stainless steel is taken into consideration with respect to its structural characteristics and structure mechanism.

Before SS 316L SPH material was introduced, SS 316L austenitic stainless steel had been considered as one of the best metallic materials for severe heat conditions. However, SS 316L SPH stainless steel was later developed from SS 316L in Europe. It is known to have better properties against irradiation and high temperature conditions, and is recently chosen as the material for structural components of a fusion reactor, for examples, NET (the next European Torus). Additionally, this material is known to have excellent properties against static creep conditions, so that it is employed as the component structural material of a FBR.

The specification of the chemical compositions of SS 316L SPH stainless steel are given in Table 2.1.3.1. The minimum 0.06 to the maximum 0.08 % of nitrogen (N) and the minimum 0.01 to the maximum 0.03 % of carbon (C) are included. Its physical properties are given in Table 2.1.3.2.

2.2 Viscoplastic Theories

2.2.1 History of the Models for Inelastic Deformation

Since it is impossible to describe correctly the inelastic behavior, many kinds of approximations for the correlation between stress and strain in the inelastic domain have been proposed. Two widely differing central assumptions to describe the inelastic behaviors are developed as follows (Ref. [2.9]) :

1) Yield condition, which separates rate-independent recoverable elastic deformation from rate-dependent nonrecoverable inelastic deformation, is assumed. Before yielding, no inelastic deformation can occur. In the detail, the principle series of works and some other theories exist which were contributed by the following authors :

Bingham, Hohenemser, Perzyna and Chaboche (main series), and

Phillips, Robinson, Eisenberg and some others.

2) Viscoplastic deformation can occur at any stress level without referring the yield condition, where elastic and inelastic deformations are treated together. Inelastic deformation can actually be observed before the yielding, whose typical example is shown in Figure 2.2.1.1. The related authors are as follows :

Valains, Bodner, Hart, Lee, Miller, Krieg, Liu, Stouffer and Walker.

In the following sections, some well-used theories for viscoplasticity will be described. These theories are based on the primitive constitutive theory, which is explained in Appendix 1, where the following assumptions stand :

1) Strain can be treated being divided into three parts i.e. elastic, inelastic and thermal strains :

$$\varepsilon_{ij} = \varepsilon^{e}_{ij} + \varepsilon^{p}_{ij} + \varepsilon^{t}_{ij}.$$

Here, thermal strain means the strain due to the natural change of size by temperature variation.

2) The material has isotropic behavior.

3) The inelastic response of material is incompressible with $\varepsilon^{p}_{kk} = 0$.

4) The hydrostatic pressure σ_{kk} of stress σ_{ij} has no influence on inelastic deformation. Therefore, all theories will work with the stress deviator defined as follows :

$$s_{ij} = \sigma_{ij} - \frac{1}{3}\sigma_{kk}\delta_{ij} \qquad (2.2.1.1)$$

2.2.2 Walker's Theory

This theory was first proposed by K. P. Walker in 1981 (Ref. [2.10], [2.11], [2.12], [2.13]).

This theory is capable of modeling the cyclic hardening and softening of hysteresis loops without considering a yield surface. Here, back stress Y and drag stress K, which are internal state variables, introduce kinematic hardening and isotropic hardening, respectively. (Miller's theory, Chaboche's theory and Robinson's theory take into consideration also these two internal state variables for hardening and softening.) As external deviatoric stress, s_{ij} is also included.

The correlation of the flow law may be written as follows :

$$\dot{\varepsilon}^{p}_{ij} = \left[\frac{\left| \frac{3}{2} s_{ij} - Y_{ij} \right|}{K} \right]^{n} \frac{\left| \frac{3}{2} s_{ij} - Y_{ij} \right|}{\left(\frac{3}{2} s_{ij} - Y_{ij} \right)} \qquad (2.2.2.1)$$

where

$$\left| \frac{3}{2} s_{ij} - Y_{ij} \right| = \sqrt{\left(\frac{3}{2} s_{ij} - Y_{ij} \right) \left(\frac{3}{2} s_{ij} - Y_{ij} \right)} \qquad (2.2.2.2)$$

Concurrently, the following hardening laws on back stress Y_{ij} and on drag stress K stand :

$$\dot{Y}_{ij} = (n_1 + n_2) \dot{\varepsilon}^{p}_{ij} + \frac{\partial n_1}{\partial T} \dot{T} \varepsilon^{p}_{ij} - (Y_{ij} - Y_{ij,0} - n_1 \varepsilon^{p}_{ij}) \left(\dot{G} - \frac{1}{n} \frac{\partial n_2}{\partial T} \dot{T} \right) \qquad (2.2.2.3)$$

$$K = K_1 - K_2 \exp (-n_7 P) \qquad (2.2.2.4)$$

where

$$\dot{G} = \{ n_3 + n_4 \exp (-n_5 P) \} \dot{P} + n_6 \left| Y_{ij} \right|^{m-1} \qquad (2.2.2.5)$$

$$P = \int d\left| \varepsilon^{p}_{ij} \right| \qquad \text{or} \qquad \dot{P} = \left| \dot{\varepsilon}^{p}_{ij} \right| \qquad (2.2.2.6)$$

Here, twelve temperature-dependent constants, n, m, n_j (j = 1 to 7), $Y_{ij,0}$, K_1 and K_2 are included. Parameter $Y_{ij,0}$ means the stress value difference in the two hysteresis tips. Under the stationary temperature condition, the following relation can be led from expressions 2.2.2.2, 2.2.2.4 and 2.2.2.5 :

$$\begin{aligned} Y_{ij} = {} & (n_1 + n_2) \dot{\varepsilon}^{p}_{ij} \\ & - \{ n_3 + n_4 \exp (-n_5 P) \} \left| \dot{\varepsilon}^{p}_{ij} \right| (Y_{ij} - Y_{ij,0} - n_1 \varepsilon^{p}_{ij}) \\ & - n_6 \left| Y_{ij} \right|^{m-1} (Y_{ij} - Y_{ij,0} - n_1 \varepsilon^{p}_{ij}) \end{aligned} \qquad (2.2.2.7)$$

The first term, the second term and the third term of the right side of expression 2.2.2.6 mean hardening, dynamic recovery and static recovery, respectively.

With the following uniaxial correlation which can be led from relation 2.2.2.1, stress-strain curve of simple tensile tests can be drawn as shown in Figure 2.2.2.1.

$$\sigma = Y + K \sqrt[n]{\dot{\varepsilon}^{p}} \qquad (2.2.2.8)$$

The corresponding correlation in Chaboche's model will be expressed in the next chapter to be compared with relation 2.2.2.8.

Primary creep, relaxation and strain rate effects are modeled with parameter n. To explain the secondary creep, the third term in expression 2.2.2.6 is essential. This theory has been found adequate for the inelastic strain rate effects during such variation range as from 10^{-6} /sec to 10^{-3} /sec, while too large stress values are predicted at higher strain rates (Ref.[2.14],[2.15]). In Figure 2.2.2.2, the results of theoretically predicted hysteresis loops for Hastelloy-X are compared

with the experimental data (Ref.[2.16]).

2.2.3 Chaboche's Theory

This viscoplastic constitutive theory originated by E. C. Bingham has recently been developed by J. L. Chaboche (Ref.[1.8], [1.9], [2.17], [2.18]).

This theory is capable of modeling the cyclic hardening and softening of hysteresis loops with considering the yield surface. Here, back stress Y_{ij} and a state variable $\hat{R}$ correlated with the yield stress introduce kinematic hardening and isotropic hardening, respectively. While constant drag stress K is responsible for strain rate sensitivity. (Walker's theory, Miller's theory and Robinson's theory also take into consideration two internal state variables for hardening and softening.) As external stress, s_{ij} is also included.

The yield law is expressed in this theory as follows :

$$F(s_{ij}, Y_{ij}, \hat{R}) = \left| \frac{2}{3} s_{ij} - Y_{ij} \right| - \hat{R} \qquad (2.2.3.1)$$

In the following flow law, this yield law is employed :

$$\dot{\varepsilon}^{p}_{ij} = \begin{cases} \left[\dfrac{F(s_{ij}, Y_{ij}, \hat{R})}{K} \right]^{n} \dfrac{\left| \frac{2}{3} s_{ij} - Y_{ij} \right|}{\left(\frac{2}{3} s_{ij} - Y_{ij} \right)} & \text{for } F > 0 \\ 0 & \text{for } F \le 0 \end{cases} \qquad (2.2.3.2)$$

Concurrently, the following hardening laws on back stress Y_{ij} and on the state variable $\hat{R}$ stand :

$$\dot{Y}_{ij} = C f(P) [A \dot{\varepsilon}^{p}_{ij} - \dot{P} Y_{ij} - B \left| Y_{ij} \right|^{m-1} Y_{ij}] + \left[\frac{1}{C} \frac{\partial C}{\partial T} + \frac{1}{A} \frac{\partial A}{\partial T} + \frac{1}{f(P)} \frac{\partial f(P)}{\partial T} \right] \dot{T} Y_{ij} \qquad (2.2.3.3)$$

$$\dot{\hat{R}} = \frac{1}{2AC} \frac{\partial f(P)}{\partial P} \frac{1}{f^{2}(P)} \left| Y_{ij} \right|^{2} \dot{P} + g(P) \dot{P} + k \qquad (2.2.3.4)$$

where

$$f(P) = m_1 + (1 - m_1) \exp (-\beta P) \qquad (2.2.3.5)$$

$$g(P) = m_2 \{ 1 - \exp (-\gamma P) \} \qquad (2.2.3.6)$$

Here, eleven temperature dependent constants, K, n, k, A, B, C, m, m_1, m_2, β and γ are included. Parameter k means the initial value of isotropic state variable $\hat{R}$.

The details of this theory will be explained in the next chapter. This theory is now confirmed to give one of the best models suited for inelastic material characteristics in a wide range. It is, however, not so appropriate to describe the tensile behavior, likely as Walker's theory, or Robinson's theory.

2.2.4 Miller's Theory

This theory was first proposed by A. Miller (Ref.[2.12], [2.19], [2.20], [2.21]), which is capable of modeling the material behavior under wide range of complicated high temperature conditions without considering the yield surface. Here, back stress Y_{ij} and drag stress K, which are internal state variables, introduce kinematic hardening and isotropic hardening, respectively. (Walker's theory, Chaboche's theory and Robinson's theory have also these two internal state variables for hardening and softening.) As external stress, s_{ij} is also included.

This theory employs hyperbolic sine function in the flow law. Only constants K_0, which is the initial value of K, and θ are dependent on temperature. The correlation of the flow law may be written as follows :

$$\dot{\varepsilon}^p_{ij} = B\theta \left[\sinh \left(\frac{\left| \frac{2}{3} s_{ij} - Y_{ij} \right|}{K} \right)^{\frac{3}{2}} \right]^n \frac{\left| \frac{2}{3} s_{ij} - Y_{ij} \right|}{\left(\frac{2}{3} s_{ij} - Y_{ij} \right)} \qquad (2.2.4.1)$$

$$\dot{Y}_{ij} = A_1 \left[\dot{\varepsilon}^p_{ij} - B\theta \{ \sinh (C_1 \left| Y_{ij} \right|) \}^n \frac{\left| Y_{ij} \right|}{Y_{ij}} \right] \qquad (2.2.4.2)$$

$$\dot{K} = A_2 \left[\left| \dot{\varepsilon}^p_{ij} \right| \left(C_2 + \left| Y_{ij} \right| - \frac{C_3 K^3}{C_1} \right) - C_2 B\theta \{ \sinh (C_3 K^3) \}^n \right] \qquad (2.2.4.3)$$

Here, $B\theta$ stands for the effective diffusion coefficient, which may be written as follows (Ref.[2.22]) :

$$D_{eff} = B\theta = B \left(\exp \left[- \frac{Q_1}{kT} \right] + C_4 \exp \left[- \frac{Q_2}{kT} \right] \right) \qquad (2.2.4.4)$$

In the theory, nine temperature independent parameters, n, A_1, A_2, B, C_1, C_2, C_3, Q_1 and Q_2 are included. The initial value of drag stress, K_0, needs to be determined as a temperature dependent constant, and T in the above expressions is temperature in °K.

The first term and the second term of expression 2.2.4.2 mean hardening and static thermal recovery, respectively, while no dynamic recovery is included in this expression. Hence, even if at high strain rates, Y_{ij} depends on inelastic strain rate $\dot{\varepsilon}^p_{ij}$. In addition, expression 2.2.4.2 suggests that back stress Y_{ij} saturates very rapidly due to the hyperbolic sine function. On the other hand, both dynamic recovery and static thermal recovery terms are presented in expression 2.2.4.3, which indicates that cyclic change in stress-strain response can be modeled not in terms of Y_{ij}, but just by K.

Tri-linear characteristics are exhibited by this theory as shown in Figure 2.2.4.1, where they consist of such three transitions as an elastic domain, an inelastic domain with Y_{ij} growing linearly and an inelastic domain with constant s_{ij}. In the inelastic domain, since inelastic strain rate becomes larger enough than elastic strain rate, the following expression can stand for governing the growth of inelastic strain as an example :

$$\sigma = Y + K \left[\sinh^{-1}\left(\frac{\dot{\varepsilon}}{B\theta}\right)^{\frac{1}{n}} \right]^{\frac{2}{3}} \qquad (2.2.4.5)$$

which is uniaxial form under a simple tensile condition. In Figure 2.2.4.2, the results of theoretically predicted cyclic loops for SS 316 stainless steel are compared with the corresponding experimental data.

2.2.5 Bodner, Partom and Stouffer's Theory

This theory is based on an assumption of small strain and that of the additive decomposition of total strain rate into elastic parts, consistent with the basic skeletal structure. The theory is different from the other theories by eliminating the concept of back stress Y_{ij}. It is, therefore, impossible to describe negative creep effects at positive stress values, negative relaxation, or an after-effect type of recovery in the material when the stress is removed.

While its general anisotropic theory has been established by Bodner and Stouffer (Ref.[2.23]) and further related works concerning the generalization of the anisotropic model by Young may be found (Ref. [2.24]) , the following isotropic form is employed in the present studies (Ref.[2.25]) :

$$\dot{\varepsilon}_{ij}^{p} = D_0 \exp\left[-\frac{1}{2}\left(\frac{Z^2}{\left| \frac{3}{2} s_{ij} \right|} \right)^{n} \right] \frac{|s_{ij}|}{s_{ij}} \qquad (2.2.5.1)$$

The inelastic flow is assumed in the direction of the deviatoric stress. Concurrently, variable Z is linearly decomposed into the sum of a directional part Z^D and an isotropic part Z^I as follows :

$$Z = Z^D + Z^I \qquad (2.2.5.2)$$

where,

$$Z^D = \beta_{ij} \frac{\sigma_{ij}}{|\sigma_{mn}|} \qquad (2.2.5.3)$$

$$\dot{Z}^I = m (Z_1 - Z^I) \dot{W}^P - A_1 Z_2 \left(\frac{Z^I - Z_2}{Z_1} \right)^{r1} \qquad (2.2.5.4)$$

The component of the directional variable Z^D in the direction of the total stress is added to the isotropic variable Z^I, which follows the hardening with the rate of plastic work W^p defined as follows :

$$\dot{W}^p = s_{ij} \dot{\varepsilon}_{ij}^{p} \qquad (2.2.5.5)$$

Directional variable β_{ij} means also hardening as follows :

$$\dot{\beta}_{ij} = m_2 \left(Z_3 \frac{|s_{ij}|}{s_{ij}} - \beta_{ij} \right) \dot{W}^p - A_2 Z^{I} \left(\frac{|\beta_{ij}|}{Z^{I}} \right)^{r_2} \frac{|\beta_{ij}|}{\beta_{ij}} \qquad (2.2.5.6)$$

Parameter Z_1 is the saturated value of variable Z^I, parameter Z_2 is the minimum value of Z^I for a particular temperature, A_i and r_i ($i = 1, 2$) are temperature-dependent material parameters, and m_1 and m_2 are a temperature-independent hardening parameter and a temperature-independent hardening rate, respectively.

Here, D_0 and n are included as other parameters. The above expressions can explain kinematic and isotropic hardening, but accurate modeling of cyclic effects require a certain function of plastic work (which is equal to one for purely isotropic hardening and equal to zero for purely kinematic hardening).

2.2.6 Hart's Theory

This theory has less importance theoretically, but is interesting historically. The theory was proposed by E. C. Hart on which the succeeding no-yield surface viscoplastic theories are based, for instance Walker's theory (Ref.[2.26]).

In this theory, two state variables are employed. One is back stress Y_{ij} and the other is hardening S which is a scalar variable. The constant parameter K can not mean isotropic hardening, so that this theory may model only kinematic hardening. Back stress Y_{ij} and stress s_{ij} are employed as internal stress and external stress, respectively.

The following expressions are employed in this theory :

$$\dot{\varepsilon}^p_{ij} = \dot{a} \left[\frac{\left| \frac{2}{3} s_{ij} - Y_{ij} \right|}{K} \right]^n \frac{\left| \frac{2}{3} s_{ij} - Y_{ij} \right|}{\left(\frac{2}{3} s_{ij} - Y_{ij} \right)} \qquad (2.2.6.1)$$

$$\dot{Y}_{ij} = K \dot{\varepsilon}_{ij} - K b \frac{S^m Y_{ij}}{|Y_{kl}| \left(\ln \frac{S}{|Y_{kl}|} \right)^{\frac{1}{\beta}}} \qquad (2.2.6.2)$$

where

$$\dot{S} = \frac{c b S^{m+1} \Gamma}{\left(\ln \frac{S}{|Y_{kl}|} \right)^{\frac{1}{\beta}}} \qquad (2.2.6.3)$$

$$\Gamma = \frac{\gamma \delta}{S} \qquad (2.2.6.4)$$

Expression 2.2.6.4 is defined in another form by Delph. (Ref.[2.27])

Back stress Y_{ij} grows linearly with inelastic strain in the initial phase, and saturates after the balance of the first term (linear hardening term) and the second term (static thermal recovery term) of the right side of expression 2.2.6.2. The saturated value of back stress is dependent only on strain rate, since no dynamic recovery is included. In expression 2.2.6.2, the static thermal recovery term grows rapidly, which suggests the same tri-linear stress-strain response characteristics as those of Miller's theory. (Ref.[2.27])

The theory includes no time-differential temperature term. Therefore, the state variable can not change during nonisothermal " elastic" excursions.

2.2.7 Robinson's Theory

Robinson has proposed a viscoplastic theory to explain thermo-mechanical history (Ref.[2.28], [2.29], [2.30]).

A certain yielding function may be written in this theory as follows :

$$F (s_{ij}, Y_{ij}, K) = \frac{\left| \frac{2}{3} s_{ij} - Y_{ij} \right|}{K} - 1 \qquad (2.2.7.1)$$

Here, parameter K, which is a scalar state variable, means something like the largeness of the yield surface as shown in Figure 2.2.7.1. Parameter K is described as follows :

$$K = K (W, T) = K_s(T) + [K_i(T) - K_s(T)] \exp \left[\frac{-W}{W_0(T)} \right] \qquad (2.2.7.2)$$

where W is the inelastic work expressed as follows :

$$W = \int \sigma_{ij} \, d \varepsilon_{ij} \qquad (2.2.7.3)$$

Here, $K_i (T) = K (0,T)$, $K_s (T) = K (\infty,T)$ and $W_0 (T)$ determine the temperature-dependent cyclic hardening rate. In this theory, the gradual hardening is assumed to be isotropic, which can be described in terms of a single scalar state variable K.

Using this function, the flow law can stand as follows :

$$\mu \dot{\varepsilon}^{p}_{ij} = \begin{cases} F (s_{ij}, Y_{ij}, K)^{\frac{n-1}{2}} \dfrac{\left| \frac{2}{3} s_{ij} - Y_{ij} \right|}{\left(\frac{2}{3} s_{ij} - Y_{ij} \right)} & \text{for } F \geq 0 \text{ and } s_{ij} \left(\frac{2}{3} s_{ij} - Y_{ij} \right) \geq 0 \\ 0 & \text{for } F < 0 \text{ or } s_{ij} \left(\frac{2}{3} s_{ij} - Y_{ij} \right) < 0 \end{cases} \qquad (2.2.7.4)$$

Where parameters μ and n are included. Back stress Y_{ij} is described in the hardening law as

follows :

$$\dot{Y}_{ij} = \begin{cases} \dfrac{H}{G^{\frac{\beta}{2}}} \dot{\varepsilon}^{p}_{ij} - R\, G^{\frac{n-\beta-1}{2}} \dfrac{|Y_{ij}|}{Y_{ij}} & \text{for } G \geq G_0 \text{ and } s_{ij} Y_{ij} \geq 0 \\ \dfrac{H}{G_0^{\frac{\beta}{2}}} \dot{\varepsilon}^{p}_{ij} - R\, G_0^{\frac{n-\beta-1}{2}} \dfrac{|Y_{ij}|}{Y_{ij}} & \text{for } G < G_0 \text{ or } s_{ij} Y_{ij} < 0 \end{cases} \qquad (2.2.7.5)$$

where

$$G = \frac{|Y_{ij}|}{K_0} \qquad (2.2.7.6)$$

Here, parameters H, R, β and G_0 are included. K_0 is the value of K at the reference temperature T_0. Kinematic features are modeled by the back stress. Parameter G_0 is a small value to avoid the occurrence of a singularity as $Y_{ij} = 0$ and causes a large change in back stress Y_{ij} on reversed loading when $s_{ij} Y_{ij} \leq 0$.

All the temperature dependence are described in the flow law, where parameters n and μ are dependent on temperature as well.

Table 2.1.1.1 : Stress behaviors on the first wall surface

	Burn time	Off burn time
σ^p at A	-200 MPa	200 MPa
σ^p at B	200 MPa	-200 MPa
σ^e at B	800 MPa	-800 MPa

Table 2.1.1.2 : Expected thermal cycles of fusion reactors

Reactors	JT-60	INTOR	Characteristics Core
Beam pulse width	2200 sec	226 sec	800 sec
Operation mode	sub-stationary	stationary	stationary
Start-up time	25 to 55 sec	3 sec	20 sec
Wall loading	< 34 W/cm^2	40 W/cm^2	30 W/cm^2
Neutron loading	88 W/cm^2	130 W/cm^2	110 W/cm^2
Duty	$\frac{1 \text{ cycle}}{2400 \text{ sec}}$	$\frac{30 \text{ cycles}}{1 \text{ day}}$	$\frac{800 \text{ sec}}{1000 \text{ sec}}$

Table 2.1.3.1 : Chemical compositions in weight percentages of SS 316L SPH stainless steel

	C	Ni	Cr	Nm	Cu	Mo	Si	Co
Min.	0.01	12.0	17.0	1.6	0.0	2.7	0.0	0.0
Max.	0.03	12.5	18.0	2.0	1.0	3.3	0.5	0.25

	P	Ta	N	B	S
Min.	0.0	0.0	0.06	0.0	0.0
Max.	0.035	0.15	0.08	0.0025	0.025

Table 2.1.3.2 : Physical properties of SS 316L SPH stainless steel

Temperature (℃)	20	300	500	700
Density (kg/m^3)	8000	7870	7780	7680
Thermal expansion ($10^{-6}/K$)	16	17	18	19
Elastic modulus (KN/mm^2)	195	175	155	140
Thermal conductivity (W/m/K)	14.5	18	20	23
Specific heat (J/kg/K)	480	550	580	600

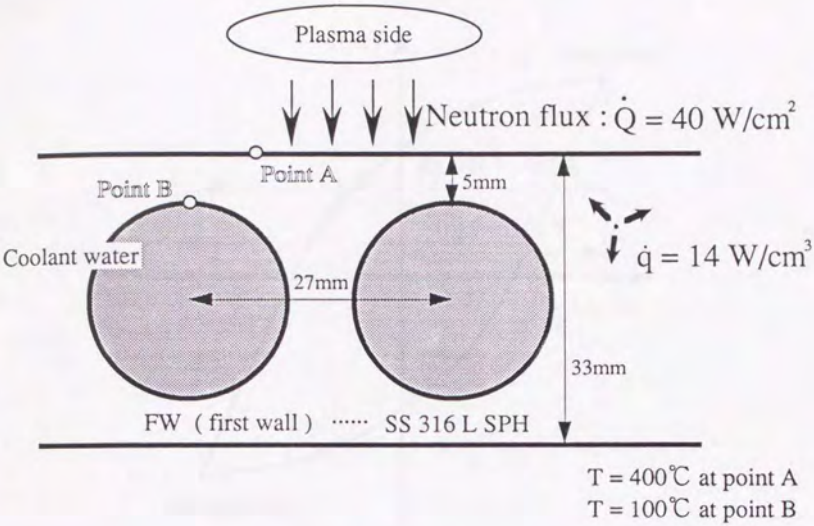

Figure 2.1.1.1 : First wall conditions (NET)

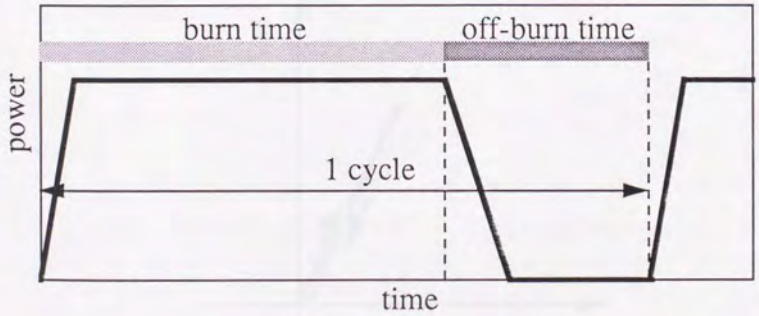

Continuous pulse operation : { 500 sec = burn time
260 sec = off-burn time

Figure 2.1.1.2 : Burning history of a typical operation (NET)

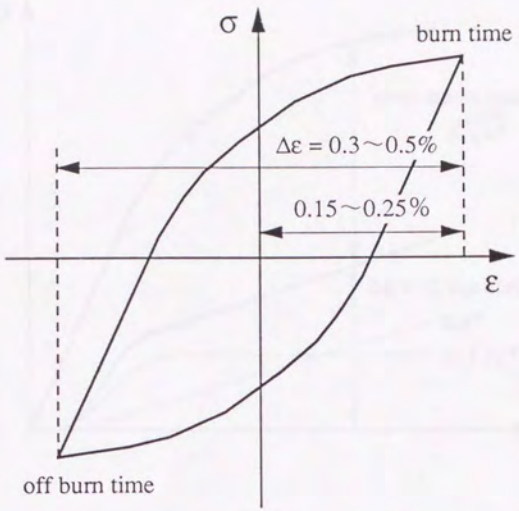

Figure 2.1.1.3 : Typical hysteresis curve during operation (NET)

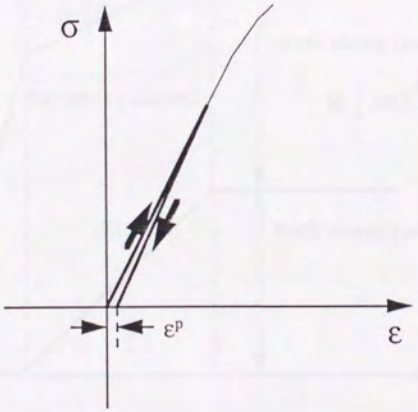

Figure 2.2.1.1 : Typical inelastic behavior before yielding (NET)

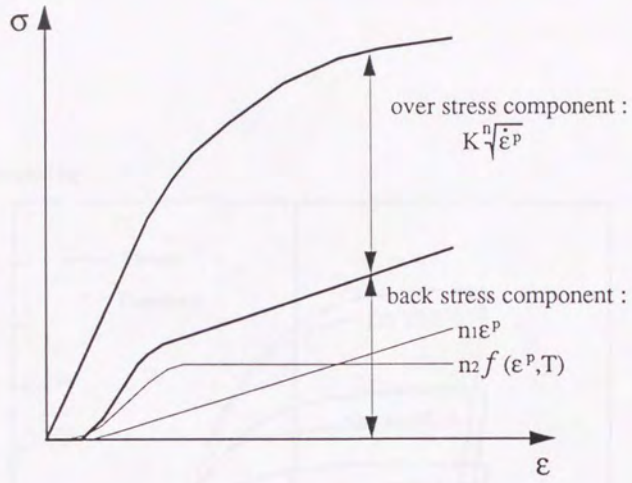

Figure 2.2.2.1 : Tensile behavior of stress components expressed by Walker's theory

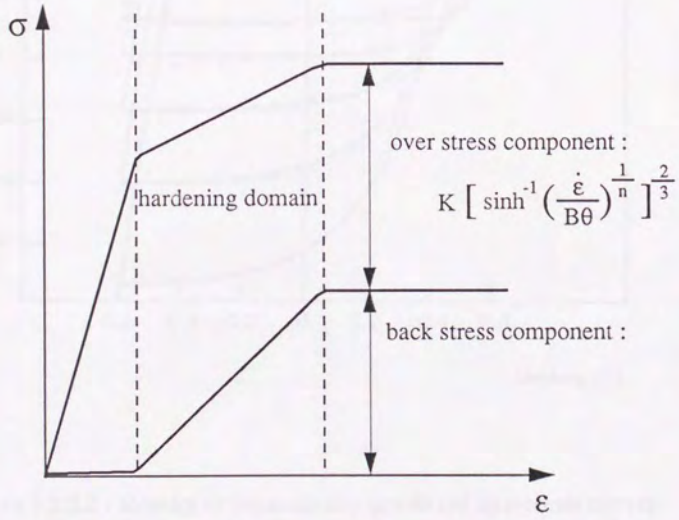

Figure 2.2.4.1 : Tensile behavior of stress components expressed by Miller's theory

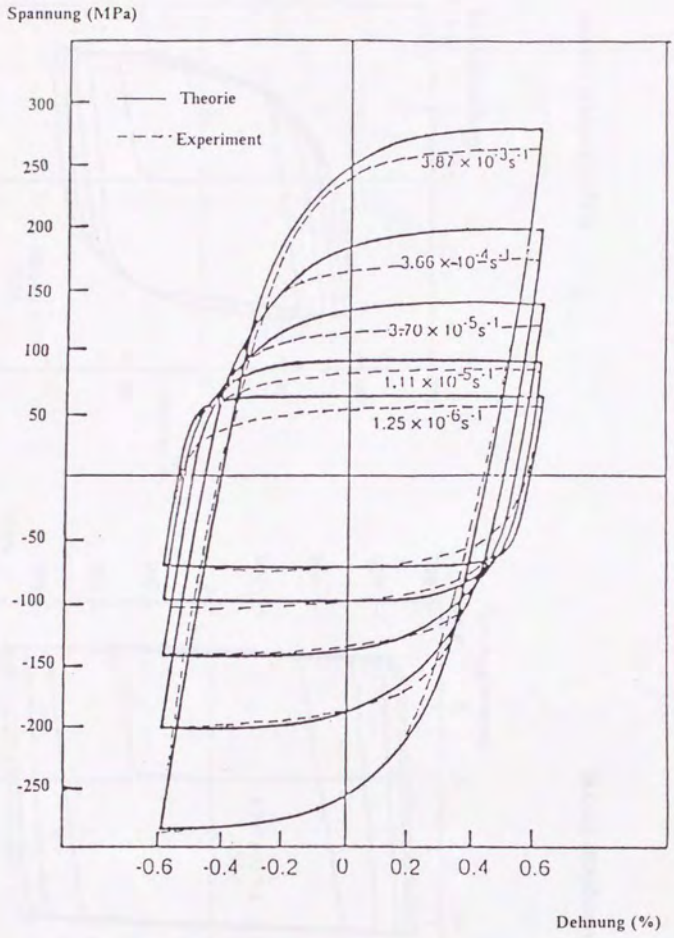

Figure 2.2.2.2 : Results of theoretically predicted hysteresis curves for Hastelloy-X compared with experimental data (Ref. [2.16])

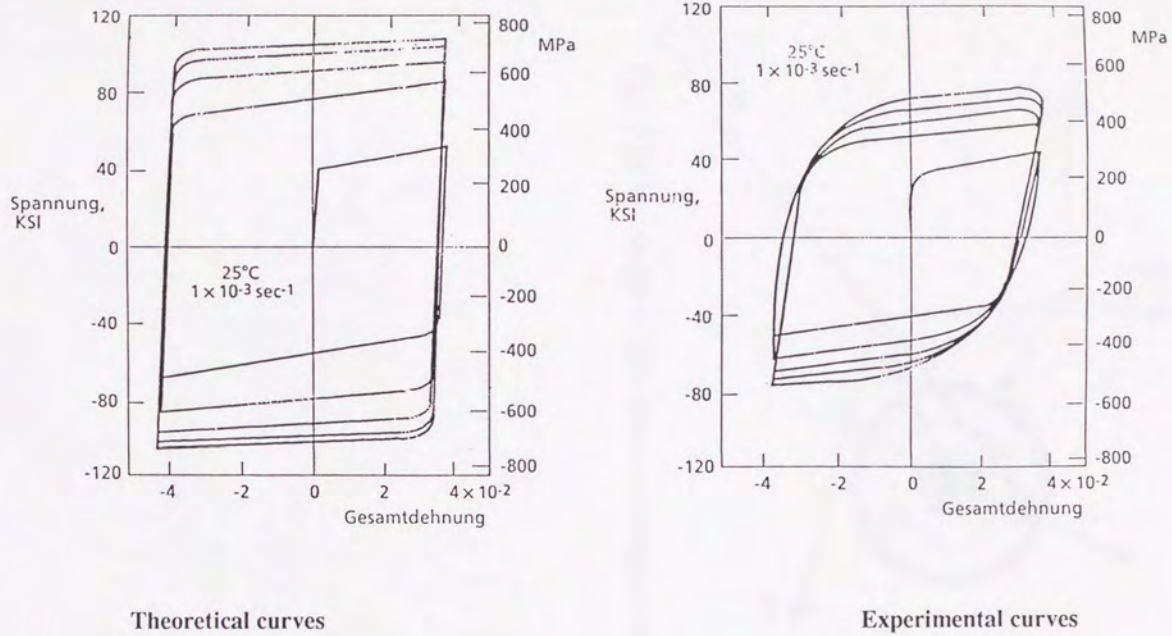

Theoretical curves **Experimental curves**

Figure 2.2.4.2 : Results of theoretically predicted hysteresis curves for SS 316 stainless steel compared with experimental data (Ref. [2.16])

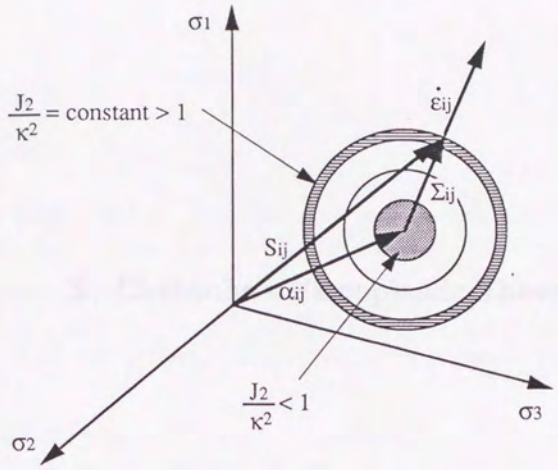

Figure 2.2.7.1 : Image of yield surface in Robinson's theory

3 Chaboche's Viscoplastic Theory

3.1 Formulations of Chaboche's Theory

3.1.1 Standard forms

As mentioned in Chapter 2, the viscoplastic theory which Chaboche has proposed is constructed under three principal assumptions, i.e., a yield function, a flow law and two hardening laws (considering isotropic hardening and dynamic hardening). State variables s_{ij}, Y_{ij}, ε^p and $\hat{R}$ are applied stress, back stress, inelastic strain and the state variable correlated with yield stress, respectively. A variable P is the accumulated inelastic strain as expressed in equation 2.2.2.6.

Eleven temperature-dependent constants, K, n, k, A, B, C, m, m_1, m_2, β and γ are included. These parameters have the units shown in Table 3.1.1.1. External stress s_{ij} corresponds to the present state, and internal stresses Y_{ij} and R are related to the load history. The first part, the second part and the third part in the first term of relation 2.2.3.3 mean hardening, dynamic recovery and static recovery, respectively.

Here, while K may be a constant, the isotropic hardening can be described by introducing a state variable R. The flow law means that no inelastic strain occurs before yielding.

3.1.2 Simplified Forms

Since it is almost impossible to controll the temperature distribution within a test specimen, and since it is difficult to determine the Chaboche's temperature-dependent parameters directly as functions of temperature, each temperature-dependent parameter could generally be expected to be found for some stationary temperature conditions one by one parametrically. To search the Chaboche's parameters, the experiments can be done more easily and reliably under fixed temperature atmosphere. Here, the last term of expression 2.2.3.3, vanishes due to non-temperature dependency at first.

Furthermore, some terms in the expressions on back stress Y and the state variable R may be reduced so as to be able to determine the experiments more simply. Secondary creep, which is caused by static recovery, can not be visible in experiments up to 400℃, and nonelevated temperature causes no kinematic time hardening recovery. Therefore, the third component of the first term of expression 2.2.3.3 vanishes (i.e., B=0). On the other hand, a function $f(P)$ of expression 2.2.3.3 is generally regarded to be constant, and a back stress-dependent term of

expression 2.2.3.4 is normally ignored. Hence, expressions 2.2.3.3 and 2.2.3.4 can be led to the following reduced forms :

$$\dot{Y}_{ij} = C [A \dot{\varepsilon}^p_{ij} - \dot{P} Y_{ij}] \qquad (3.1.2.1)$$

$$\hat{R} = g(P) + k = (m_2 + k) - m_2 \exp(-\gamma P) \qquad (3.1.2.2)$$

It is clear that parameter k means the initial value of R when P = 0. The differential form of expression 3.1.2.2 is as follows :

$$\frac{d\hat{R}}{dP} = \gamma (m_2 + k - \hat{R}) \qquad (3.1.2.2')$$

In some literatures, parameter Q is denoted as ($m_2 + k$).

After these approximations, the number of the parameters to be determined is reduced to seven, K, n, A, C, m_2, k and γ. These expressions are very commonly used.

3.1.3 Uniaxial Forms

Under a uniaxial stress loading condition, the use of a yield surface permits isotropic hardening to be modeled by the increase in the size of a yield surface rather than by that in drag stress K. Hence, the following simple expressions are reduced from expressions 2.2.3.1 to 2.2.3.4 :

1. yield function

$$F = |\sigma - Y| - R \qquad (3.1.3.1)$$

2. flow law

$$\dot{\varepsilon}^p = \begin{cases} \left(\dfrac{|\sigma - Y| - R}{K} \right)^n \dfrac{|\sigma - Y|}{\sigma - Y} & \text{for } F > 0 \\ 0 & \text{for } F \le 0 \end{cases} \qquad (3.1.3.2)$$

3. hardening law

$$\dot{Y} = H \dot{\varepsilon}^p - D Y |\dot{\varepsilon}^p| \qquad (3.1.3.3)$$

$$\dot{R} = (h - d R) |\dot{\varepsilon}^p| \qquad (3.1.3.4)$$

where state variables σ, ε^p and Y are uniaxial stress, uniaxial inelastic strain and uniaxial back stress, respectively. A parameter R stands for uniaxial yield stress the value of which is different form that of $\hat{R}$ in expression 3.1.2.2, where new notations H, D, h and d denote ($A \times C$), C, $\gamma \times (m_2 + k)$ and γ, respectively. Here, these parameters have the units as shown in Table

3.1.3.1. The accumulated strain can be written as follows :

$$\dot{p} = |\dot{\varepsilon}^p| = \frac{3}{\sqrt{2}}\dot{P} \qquad (3.1.3.5)$$

where, state variables p and P mean the accumulated inelastic strain rates in a uniaxial field and in a multiaxial field, respectively.

3.2 Physical Interpretation of Uniaxial Assumption

3.2.1 Objectives of This Section

Since the uniaxial forms are employed and their parameters are predicted to be applied to the lifetime calculation later, their physical interpretation is given in this section. At first, each stress component of Y (back stress), R (yield stress) and Z (over stress) is displayed one by one, and then total stress is exhibited. In any case, the easiest form described in section 3.1.3 is discussed.

Expression 2.2.2.8 will be referred to be compared, in which only Y and Z are included.

3.2.2 Behavior of Back Stress

Back stress Y is the equilibrium internal stress which is changed following the inelastic dislocation of material to describe inelastic balance between the external work and the internal status. Thus, back stress is sometimes called equilibrium stress or rest stress.

Back stress expressed with expression 3.1.3.3 is dependent on only inelastic strain rate under uniaxial and stationary temperature conditions. When the integration over this expression is made, the behavior of the back stress under cyclic loading condition must be led. The integration should be done divided into two different loading processes, the case of $\varepsilon^p \geq 0$ and the case of $\varepsilon^p \leq 0$, as follows :

$$dY = (H - DY)\, d\varepsilon^p \qquad \text{for } \varepsilon^p \geq 0 \qquad (3.2.2.1a)$$

$$dY = (H + DY)\, d\varepsilon^p \qquad \text{for } \varepsilon^p \leq 0 \qquad (3.2.2.1b)$$

The former and the latter cases are called Case 1 and Case 2, respectively. On each case, the integration is carried out as fallows :

Case 1. $\dfrac{dY}{H - DY} = d\varepsilon^p$

$$\int \frac{dY}{H - DY} = \int d\varepsilon^p$$

$$-\frac{1}{D} \ln|H - DY| = \varepsilon^p + C_1$$

$$\ln|H - DY| = -D(\varepsilon^p + C_1) \qquad (3.2.2.2a)$$

Case 2. $\dfrac{dY}{H + DY} = d\varepsilon^p$

$$\int \frac{dY}{H + DY} = \int d\varepsilon^p$$

$$\frac{1}{D} \ln|H + DY| = \varepsilon^p + C_2$$

$$\ln|H + DY| = D(\varepsilon^p + C_2) \qquad (3.2.2.2b)$$

Here, C_1 and C_2 are the integration constants. These relations are shown in Figures 3.2.2.1 and 3.2.2.2, respectively. Each case has the curve for $(H \pm DY) \geq 0$ or for $(H \pm DY) \leq 0$. On the other hand, every physical phenomenon occurs with the initial value of back stress Y being equal to zero at the beginning. Additionally, such phenomena must not occur as the back stress Y increases or decreases when inelastic strain ε^p decreases or increases. Hence, the following two possibilities may actually be allowed :

$$\ln(H - DY) = -D(\varepsilon^p + C_1) \qquad \text{for Case 1} \qquad (3.2.2.3a)$$

$$\ln(H + DY) = D(\varepsilon^p + C_2) \qquad \text{for Case 2} \qquad (3.2.2.3b)$$

Furthermore, since the actual phenomena of cyclic tests give symmetric results in stress-strain curves on the zero point O after sufficient number of cycles, these constants should be related as follows in the asymptotic case :

$$\frac{\ln H}{D} + C_2 = -\left[-\frac{\ln H}{D} C_1\right] \qquad \text{for } Y = 0$$

$$\therefore\ C_1 = C_2 = C \qquad (3.2.2.4)$$

Therefore, Figure 3.2.2.3 can be led. These two exponential curves have the cross points at $\pm\varepsilon_a$ of the inelastic strain.

3.2.3 Behavior of Yield Stress

Yield stress R has some relationship with dislocation density, and R is essentially the isotropic hardening state variable. Chaboche's theory suggests expression 3.1.3.4 for yield stress R under uniaxial and stationary temperature conditions.

The integral form can be led as follows :

$$\ln\left| h - d\,R \right| = - d \int d\left| \varepsilon^{p} \right| \qquad (3.2.3.1)$$

The yield stress R, which is an isotropic hardening stress variable, always increases with the increase in accumulated inelastic strain P (equal to the integral part of the right side of expression 3.2.3.1). Hence, the curve shown in Figure 3.2.3.1 must be chosen. Of course, the yield stress R can be defined when the accumulated inelastic strain is positive.

Under the cyclic loading condition shown in Figure 3.2.3.2, the relationship between yield stress R and inelastic strain ε^{p} can be drawn as in Figure 3.2.3.3. Yield stress is constant throughout every elastic domain, 1, 3 or 5, while it increases throughout every inelastic domain, 2, 4 or 6.

3.2.4 Behavior of Over Stress

Chaboche's theory suggests that the component of stress, which dose not include back stress and yield stress, is dependent on inelastic strain rate $\dot{\varepsilon}^{p}$. The following expression on the stress component Z can be written with Chaboche's parameters K and n under uniaxial and stationary temperature conditions :

$$Z = K \sqrt[n]{\left| \dot{\varepsilon}^{p} \right|} \frac{\left| \dot{\varepsilon}^{p} \right|}{\dot{\varepsilon}^{p}} \qquad (3.2.4.1)$$

This component is called over stress.

It is too difficult to visualize these material parameters K and n. while the relationship between inelastic strain rate $\dot{\varepsilon}^{p}$ and over stress Z is shown in Figure 3.2.4.1. In this curve, parameters K and n are considered to inform the dependency of inelastic strain rate $\dot{\varepsilon}^{p}$ on over stress stress Z that is the curvature of the curve shown in Figure 3.2.4.1. With example parameter values of K = 100, n = 3.5 and K = 200, n = 5.0, the simulated over stress curves are drawn in Figure 3.2.4.2.

3.2.5 Total Stress Behaviors

In the present studies, cyclic loading tests and relaxation tests were carried out, so that the total

stress behaviors throughout these tests should be explained. Total stress σ consists of the three components as mentioned above for $\varepsilon^p \neq 0$. Total stress is expressed as follows :

$$\sigma = Y + (R + K\sqrt[n]{|\dot{\varepsilon}^p|}) \frac{|\dot{\varepsilon}^p|}{\dot{\varepsilon}^p} \qquad (3.2.5.1)$$

which is led from expression 3.1.3.2. As a reference, total stress which is expressed based on Walker's constitutive theory is expressed as follows :

$$\sigma = Y + K\sqrt[n]{|\dot{\varepsilon}^p|} \frac{|\dot{\varepsilon}^p|}{\dot{\varepsilon}^p} \qquad (3.2.5.2)$$

which is a uniaxial form.

At first, in the case of the first quarter cycle of cyclic tests or simple tensile tests, the behavior of total stress is shown in Figure 3.2.5.1. Here, the tensile loading is continued and the strain value exceeds a certain value of ε_a. Then, the value of over stress Z becomes constant, since $\dot{\varepsilon}^p$ becomes constant. It is actually difficult to measure the initial yield stress R_0. Generally, it can be measured at point $R_{p\,0.2}$ where the inelastic strain is around 0.2% of the total strain shown in Figure 3.2.5.2. Creep deformation, however, occurs as shown in Figure 3.2.5.3, before point $R_{p\,0.01}$. It may be that the elastic and the inelastic deformations appear concurrently at anytime.

Next, for the case of the last cycle of a cyclic loading test after saturation and a succeeding relaxation test, the behavior of the total stress is shown in Figure 3.2.5.4. Here, yield stress R has already been saturated to be constant through whole succeeding relaxation tests. The saturated value of yield stress R, is equal to the value of h", which is defined as follows :

$$h'' = \frac{h}{d} \qquad (3.2.5.3)$$

The behavior of back stress Y from the last cycle of a cyclic test to the end of a relaxation test is shown in Figure 3.2.5.5, which shows a little more complicated behavior. The variation goes along the curve $[\ \ln(H - D Y)\ ] = -D (\varepsilon^p + C)$ after the relaxation test. On the cyclic tests, the maximum and the minimum values of back stress $\pm Y_e$ are at the tips of the last cycle where the value of inelastic strain is $\pm \varepsilon_e$. For inelastic strain does not increase unlimitedly but should be limited under the value of ε^p_s which is defined as follows :

$$\varepsilon^p_s = \varepsilon_h - \frac{\sigma_s}{E} \qquad (3.2.5.4)$$

where ε_h is a hold strain value. Thus, the final value of back stress Y in the relaxation tests is (not saturated but) almost constant without continuously increasing up to the value of H' defined as follows :

$$H' = \frac{H}{D} \qquad (3.2.5.5)$$

which is the saturated value of the curve $[\ \ln(H - D Y)\ ] = -D (\varepsilon^p + C)$.

3.3 Behavior Simulation based on Chaboche's Model

3.3.1 Objectives of the Simulation

In this section, the material behaviors occurring through the employed experimental time history (see Chapter 4), for examples, a simple tensile curve, a cyclic hysteresis curve, a cyclic strain hardening curve and a relaxation curve, were drawn based on the uniaxial and stationary temperature forms of Chaboche's constitutive equations with different parameter sets. To search the influence of each parameter included in the equations to these material behaviors, the parameter set to simulate the material behaviors were varied parametrically.

The simulation results will be referred to the parameter identification which is described in Chapters 5 and 6, to modify the parameter values. Through the numerical procedure of parameter identification, the simulation results will be used as the basic data for handling the parameter values during the procedures to confirm the material significance on the parameter set (see Chapter 5). Through the neural procedure of parameter identification, the simulation results will be used as the training data to predict the parameter values (see Chapter 6). The results are expected to be kept as experiences in a computer memory and their references to evaluate parameter values are desired to be carried out automatically in the future, while the simulation results will be referred manually in the present studies.

3.3.2 Simulation Procedures and Program

For the simulation, a newly produced numerical program based on FORTRAN was used. This program with a certain set of parameter values as inputs can simulate the corresponding material behavior based on the uniaxial and stationary temperature form of Chaboche's constitutive equations 3.1.3.1 to 3.1.3.4. The state variables related with stress and strain, for examples, stress σ, back stress Y, yield stress R, total strain ε, elastic strain ε^e and inelastic strain ε^p can be calculated following a small time increment of $\Delta t = 0.5 \times 10^{-5}$ sec. The simulation was carried out on an IBM computer. The simulation results were recorded numerically onto floppy disks. The loading history as shown in Figure 3.3.2.1 was employed, where, except for the cases of cyclic hardening and creep simulation, strain rate $\dot{\varepsilon}$ and strain range $\Delta\varepsilon$ were kept at 2.0×10^{-4} /sec and 0.4%, respectively, and the final cycle number was 60 followed by the succeeding relaxation simulation of 2 minutes.

The sampled parameter sets to simulate the behaviors are shown in Table 3.3.2.1, where the parameter set of K = 100, n = 3.5, H = 150000, D = 1500, h' = 120, d = 3.5, k = 80 is the reference parameter set. A set of level means the magnitude of each parameter value, where level 5 is the center value which is the same to the reference value, and level 1 and level 9 are the minimum and the maximum values, respectively. Parameter values of K, n, H, D, h', d and k were shifted over the ranges of 50 to 150, 1.0 to 6.0, 50000 to 250000, 500 to 2500, -10 to 90, 1.0 to 6.0 and 40 to 120, respectively. The variable h' has been defined in the following expression 3.2.5.3, and employed as the new parameter suggesting the increment of an isotropic hardening value from the beginning (k) to the saturation point (h") instead of the original parameter h to see more clearly the characteristics of parameter set :

$$h' = h'' - k = \frac{h}{d} - k \qquad (3.3.2.1)$$

Each parameter was shifted one by one from its reference value, and the influence of each parameter to material behaviors was finally discussed. Elsewhere, the simulation results employing other parameter sets shown in Table 3.3.2.2, where only sets of level are exhibited instead of the parameter values, will be necessary to evaluate more accurate parameter sets by means of a neural procedure for parameter identification method as described in Chapter 6, while the simulated curves and the related discussions (see Chapter 8) are omitted in this chapter.

3.3.3 Simulation Results

For cyclic loading simulations, the results on each parameter variation are shown in Figure 3.3.3.1 to 3.3.3.7, respectively. It was confirmed that a cyclic hysteresis behavior is affected by all the parameters, while parameters n, H and D are dominantly effective to the cyclic hysteresis behavior.

For simple tensile simulations, the results on each parameter variation are shown in Figure 3.3.3.8 to 3.3.3.12, respectively. It was confirmed that a simple tensile behavior is mainly affected by parameters H, D and k, while the influence of parameters h' and d to the simple tensile behavior can be ignored.

For cyclic strain hardening simulations, the results on each parameter variation are shown in Figure 3.3.3.13 to 3.3.3.17, respectively. It was confirmed that a cyclic strain hardening behavior is mainly affected by parameters h, d and k, while the influence of parameters K and n to the cyclic strain hardening behavior can be ignored .

For relaxation simulations, the results on each parameter variation are shown in Figure 3.3.3.18 to 3.3.3.21, respectively. It was confirmed that a relaxation behavior is mainly affected by parameters K and n, while the influence of parameters h', d and h to the relaxation behavior can be ignored .

As a reference, the simulation of cyclic hardening and creep behaviors were carried out to suggest the parameter dependency on behaviors as shown in Table 3.3.3.1. In the cyclic hardening

simulations, strain ranges $\Delta\varepsilon$ of 0.4%, 0.6%, 0.8% and 1.0% were employed, and strain rate $\dot{\varepsilon}$ was fixed at 2.0×10^{-4} /sec. In the creep simulations, holding stress value was fixed at 200 MPa. The important points for each simulation are explained as follows :

1) cyclic hardening simulation ;

the value of saturation stress, strain range dependency (the curvature)

2) creep simulation ;

the starting point of the secondary creep (ε_b in Figure 3.3.3.22),

the steepness of the secondary creep curve, the curvature until the secondary creep

All the parameters are effective to these behaviors.

Table 3.1.1.1 : Units for the parameters included
in Standard Chaboche's constitutive equations

K	n	A	C	m_2	k	γ
N/sec	-	N	-	N	N	-

B	m	m_1	β
-	-	N	-

Table 3.1.3.1 : Units for the parameters included
in uniaxial Chaboche's constitutive equations

K	n	H	D	h	k	d
N/sec	-	N	-	N	N	-

Table3.3.2.1 : Employed parameter sets for the simulations

Set name	values							Set of level						
	K	n	H	D	k	h'	d	K	n	H	D	k	h'	d
00	100	3.5	150,000	1,500	80	40	3.5	5	5	5	5	5	5	5
K1	50	3.5	150,000	1,500	80	40	3.5	1	5	5	5	5	5	5
K2	60	3.5	150,000	1,500	80	40	3.5	2	5	5	5	5	5	5
K4	80	3.5	150,000	1,500	80	40	3.5	4	5	5	5	5	5	5
K6	120	3.5	150,000	1,500	80	40	3.5	6	5	5	5	5	5	5
K8	140	3.5	150,000	1,500	80	40	3.5	8	5	5	5	5	5	5
K9	150	3.5	150,000	1,500	80	40	3.5	9	5	5	5	5	5	5
N1	50	1.0	150,000	1,500	80	40	3.5	5	1	5	5	5	5	5
N2	50	1.7	150,000	1,500	80	40	3.5	5	2	5	5	5	5	5
N4	50	2.5	150,000	1,500	80	40	3.5	5	4	5	5	5	5	5
N6	50	4.5	150,000	1,500	80	40	3.5	5	6	5	5	5	5	5
N8	50	5.5	150,000	1,500	80	40	3.5	5	8	5	5	5	5	5
N9	50	6.0	150,000	1,500	80	40	3.5	5	9	5	5	5	5	5
H1	50	3.5	50,000	1,500	80	40	3.5	5	5	1	5	5	5	5
H2	50	3.5	70,000	1,500	80	40	3.5	5	5	2	5	5	5	5
H4	50	3.5	110,000	1,500	80	40	3.5	5	5	4	5	5	5	5
H6	50	3.5	190,000	1,500	80	40	3.5	5	5	6	5	5	5	5
H8	50	3.5	230,000	1,500	80	40	3.5	5	5	8	5	5	5	5
H9	50	3.5	250,000	1,500	80	40	3.5	5	5	9	5	5	5	5
D1	50	3.5	150,000	500	80	40	3.5	5	5	5	1	5	5	5
D2	50	3.5	150,000	700	80	40	3.5	5	5	5	2	5	5	5
D4	50	3.5	150,000	1,100	80	40	3.5	5	5	5	4	5	5	5
D6	50	3.5	150,000	1,900	80	40	3.5	5	5	5	6	5	5	5
D8	50	3.5	150,000	2,300	80	40	3.5	5	5	5	8	5	5	5
D9	50	3.5	150,000	2,500	80	40	3.5	5	5	5	9	5	5	5
L1	50	3.5	150,000	1,500	40	40	3.5	5	5	5	5	1	5	5
L2	50	3.5	150,000	1,500	50	40	3.5	5	5	5	5	2	5	5
L4	50	3.5	150,000	1,500	65	40	3.5	5	5	5	5	4	5	5
L6	50	3.5	150,000	1,500	95	40	3.5	5	5	5	5	6	5	5
L8	50	3.5	150,000	1,500	110	40	3.5	5	5	5	5	8	5	5
L9	50	3.5	150,000	1,500	120	40	3.5	5	5	5	5	9	5	5
I1	50	3.5	150,000	1,500	80	-10	3.5	5	5	5	5	5	1	5
I2	50	3.5	150,000	1,500	80	0	3.5	5	5	5	5	5	2	5
I4	50	3.5	150,000	1,500	80	20	3.5	5	5	5	5	5	4	5
I6	50	3.5	150,000	1,500	80	60	3.5	5	5	5	5	5	6	5
I8	50	3.5	150,000	1,500	80	80	3.5	5	5	5	5	5	8	5
I9	50	3.5	150,000	1,500	80	90	3.5	5	5	5	5	5	9	5
E1	50	3.5	150,000	1,500	80	40	1.0	5	5	5	5	5	5	1
E2	50	3.5	150,000	1,500	80	40	1.5	5	5	5	5	5	5	2
E4	50	3.5	150,000	1,500	80	40	2.5	5	5	5	5	5	5	4
E6	50	3.5	150,000	1,500	80	40	4.5	5	5	5	5	5	5	6
E8	50	3.5	150,000	1,500	80	40	5.5	5	5	5	5	5	5	8
E9	50	3.5	150,000	1,500	80	40	6.0	5	5	5	5	5	5	9

Table 3.3.2.2 : Additional parameter sets for identification by a neural method in set of level, 1 to 9

Patterns 1 , Addittional parameter sets for the both temperature cases
( ) means parameter sets being included in Table 3.3.2.1

	K	n	H	D	h'	d	k		K	n	H	D	h'	d	k		K	n	H	D	h'	d	k	
	1	1	5	5	5	5	5		5	5	1	1	5	5	5		5	5	5	5	1	1	5	
	1	2	5	5	5	5	5		5	5	1	2	5	5	5		5	5	5	5	1	2	5	
(	1	5	5	5	5	5	5	) (	5	5	1	5	5	5	5	) (	5	5	5	5	1	5	5	)
	1	8	5	5	5	5	5		5	5	1	8	5	5	5		5	5	5	5	1	8	5	
	1	9	5	5	5	5	5		5	5	1	9	5	5	5		5	5	5	5	1	9	5	
	2	1	5	5	5	5	5		5	5	2	1	5	5	5		5	5	5	5	2	1	5	
	2	2	5	5	5	5	5		5	5	2	2	5	5	5		5	5	5	5	2	2	5	
(	2	5	5	5	5	5	5	) (	5	5	2	5	5	5	5	) (	5	5	5	5	2	5	5	)
	2	8	5	5	5	5	5		5	5	2	8	5	5	5		5	5	5	5	2	8	5	
	2	9	5	5	5	5	5		5	5	2	9	5	5	5		5	5	5	5	2	9	5	
(	5	1	5	5	5	5	5	) (	5	5	5	1	5	5	5	) (	5	5	5	5	5	1	5	)
(	5	2	5	5	5	5	5	) (	5	5	5	2	5	5	5	) (	5	5	5	5	5	2	5	)
(	5	5	5	5	5	5	5	) (	5	5	5	5	5	5	5	) (	5	5	5	5	5	5	5	)
(	5	8	5	5	5	5	5	) (	5	5	5	8	5	5	5	) (	5	5	5	5	5	8	5	)
(	5	9	5	5	5	5	5	) (	5	5	5	9	5	5	5	) (	5	5	5	5	5	9	5	)
	8	1	5	5	5	5	5		5	5	8	1	5	5	5		5	5	5	5	8	1	5	
	8	2	5	5	5	5	5		5	5	8	2	5	5	5		5	5	5	5	8	2	5	
(	8	5	5	5	5	5	5	) (	5	5	8	5	5	5	5	) (	5	5	5	5	8	5	5	)
	8	8	5	5	5	5	5		5	5	8	8	5	5	5		5	5	5	5	8	8	5	
	8	9	5	5	5	5	5		5	5	8	9	5	5	5		5	5	5	5	8	9	5	
	9	1	5	5	5	5	5		5	5	9	1	5	5	5		5	5	5	5	9	1	5	
	9	2	5	5	5	5	5		5	5	9	2	5	5	5		5	5	5	5	9	2	5	
(	9	5	5	5	5	5	5	) (	5	5	9	5	5	5	5	) (	5	5	5	5	9	5	5	)
	9	8	5	5	5	5	5		5	5	9	8	5	5	5		5	5	5	5	9	8	5	
	9	9	5	5	5	5	5		5	5	9	9	5	5	5		5	5	5	5	9	9	5	

Patterns 2 , Additional parameter sets being dependent on temperature

in the case of T = 200℃

K	n	H	D	h'	d	k
2	8	8	8	2	2	2
2	8	8	8	2	8	8
2	8	8	8	8	2	8
2	8	8	2	2	2	8
2	8	2	8	2	2	8
2	2	8	8	2	2	8
8	8	8	8	2	2	8

in the case of T = 400℃

K	n	H	D	h'	d	k
8	2	2	2	8	8	8
8	2	2	2	8	2	2
8	2	2	2	2	8	2
8	2	2	8	8	8	2
8	2	8	2	8	8	2
8	8	2	2	8	8	2
2	2	2	2	8	8	2

Table 3.3.3.1 : Influence of each parameter to cyclic hardening behavior
(corresponding to the increase in each parameter value)

	Value of saturation stress	Strain range dependency
K	slightly up	-
n	slightly up	-
H	up	a little
D	down	large
h'	up	-
d	-	-
k	-	-

Table 3.3.3.2 : Influence of each parameter to creep behavior
(corresponding to the increase in each parameter value)

	ε_b value	steepness of the secondary creep curve	Curvature between the primary and secondary creep
K	slightly down	slightly down	slightly more steep
n	slightly down	slightly down	slightly more steep
H	down	-	-
D	considerably up	-	-
h'	down	slightly down	slightly more steep
d	down non-linearly	slightly down	-
k	considerably down	-	-

Figure 3.2.2.1 : The theoretical possibilities of back stress behavior
(case 1)

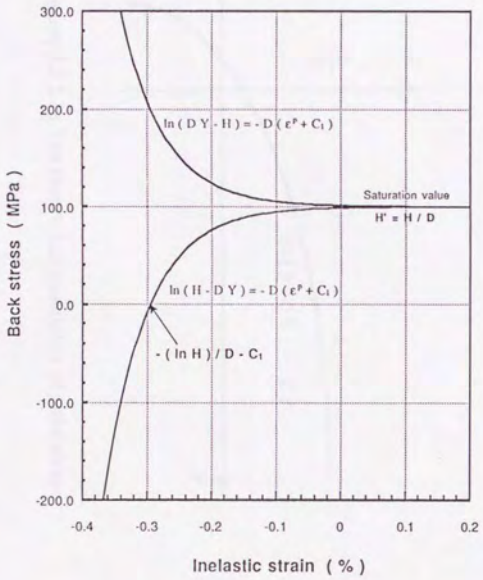

Fig.3.2.2.2 : The theoretical possibilities of back stress behavior
(case 2)

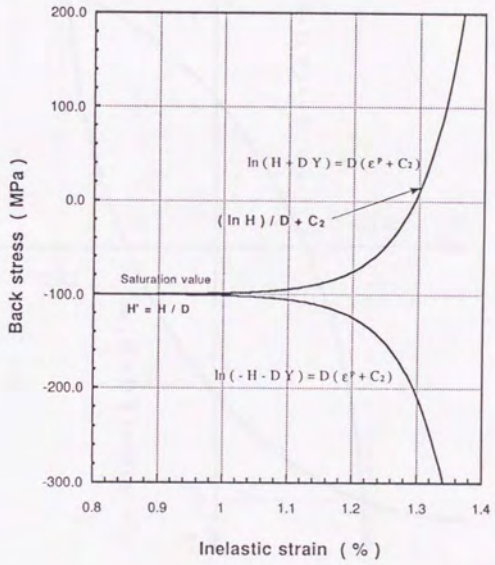

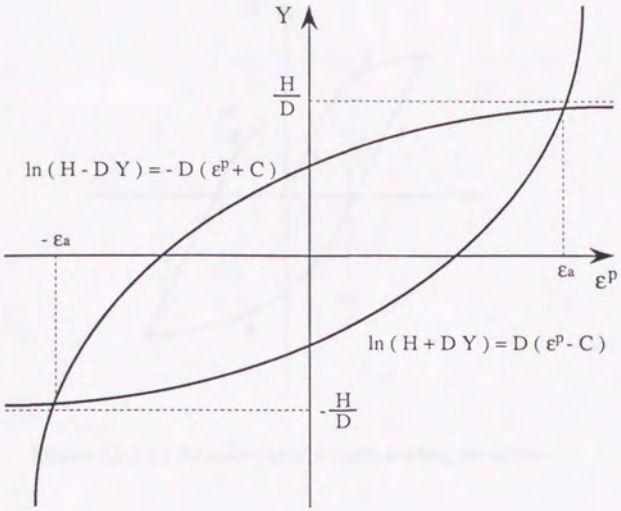

Figure 3.2.2.3 : The theoretical possibility of back stress behavior during a cyclic loading condition

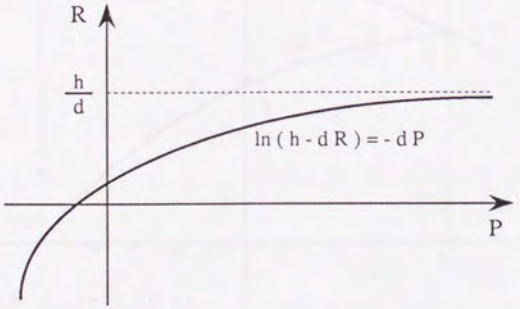

Figure 3.2.3.1 : The theoretical possibility of yield stress

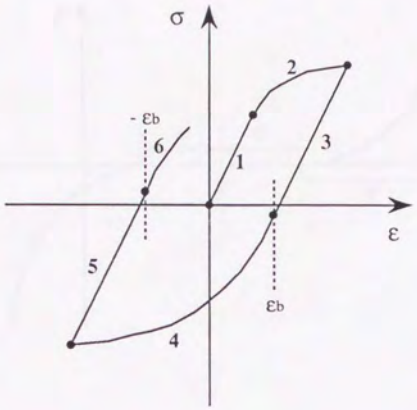

Figure 3.2.3.2 : An example of a cyclic loading condition

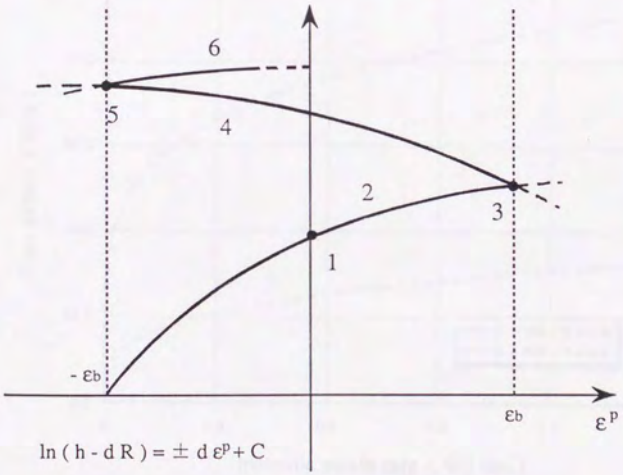

Figure 3.2.3.3 : The theoretical yield stress history
during the cyclic condition shown in Figure 3.2.3.2

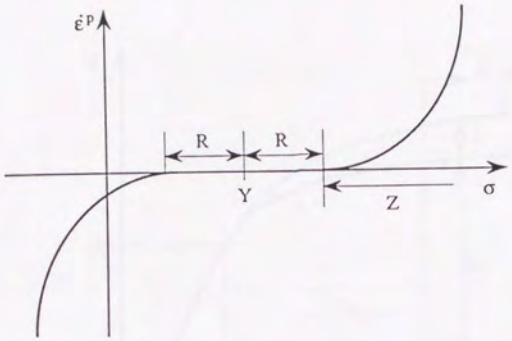

Figure 3.2.4.1 : Relation between inelastic strain rate and stress

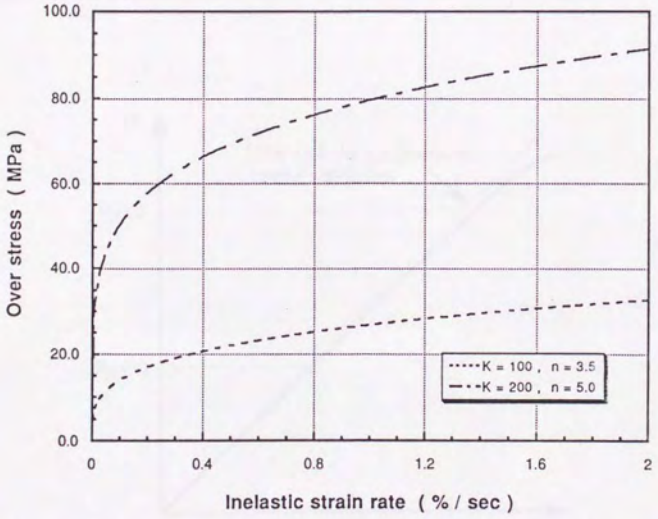

Figure 3.2.4.2 : Examples of over stress curves

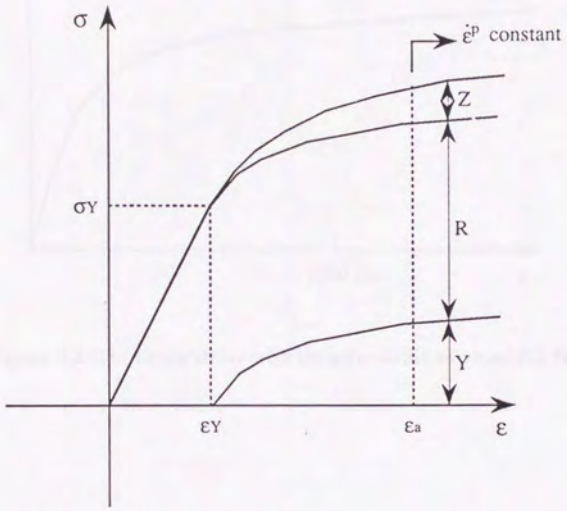

Figure 3.2.5.1 : Theoretical behavior of stress components during tensile behavior

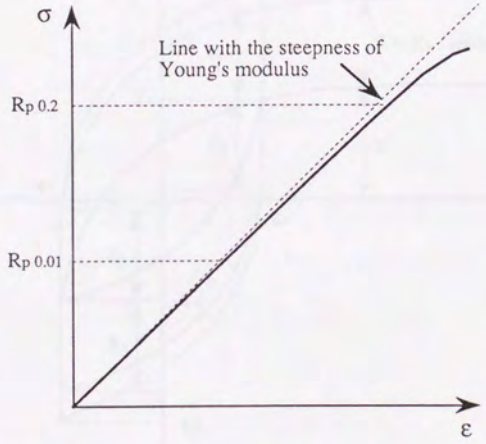

Figure 3.2.5.2 : The real experimental curve and points of $R_{p\ 0.2}$ and $R_{p\ 0.01}$

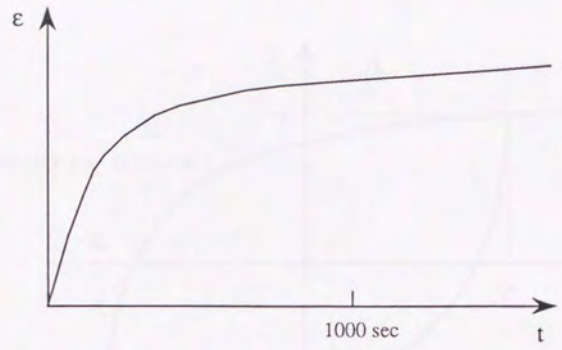

Figure 3.2.5.3 : Creep curve with inelastic strain of about 0.2 %

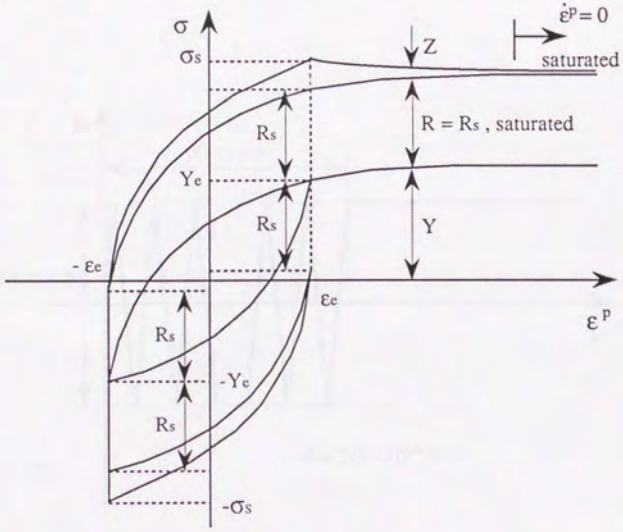

Figure 3.2.5.4 : Behavior of stress components
at the end of a cyclic test and the beginning of a relaxation test

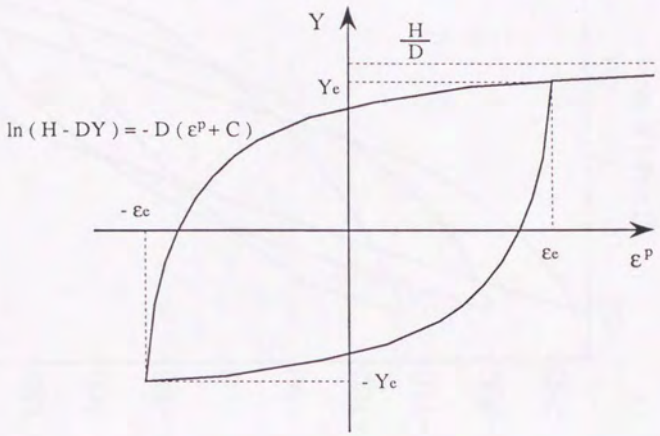

Figure 3.2.5.5 : Back stress behavior at the end of a cyclic test and the beginning of a relaxation test

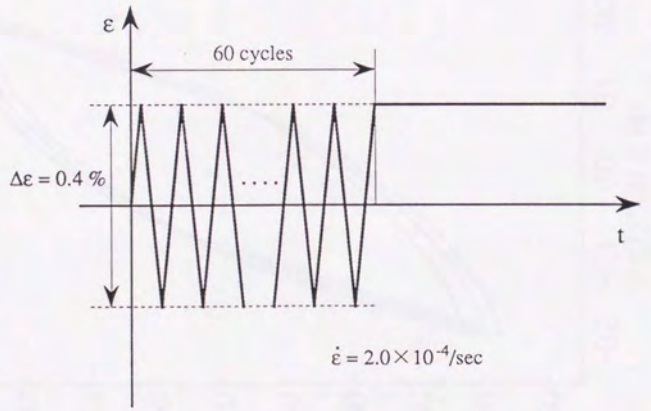

Figure 3.3.2.1 : Simulated loading history

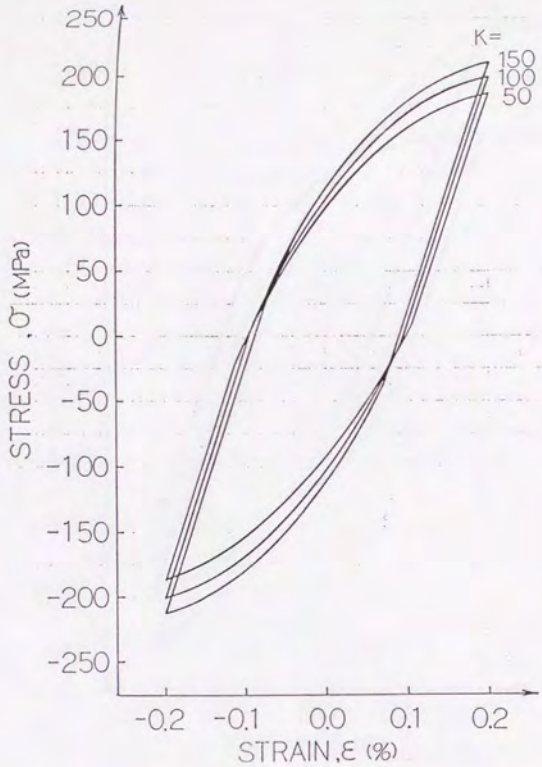

Figure 3.3.3.1 : Influence of the parameter K on the simulated cyclic behaviors

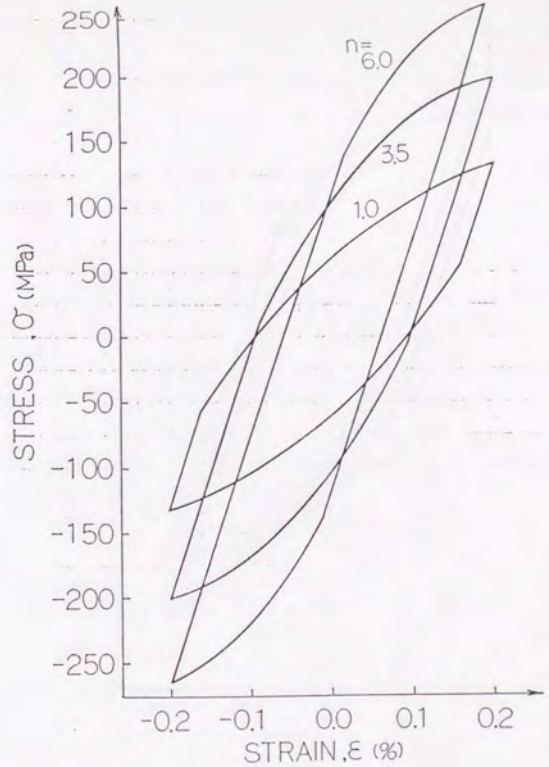

Figure 3.3.3.2 : Influence of the parameter n on the simulated cyclic behaviors

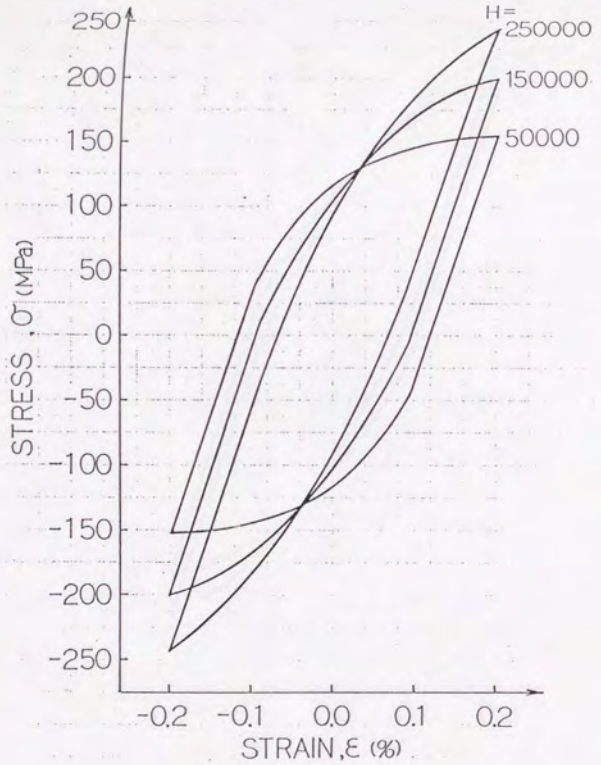

Figure 3.3.3.3 : Influence of the parameter H on the simulated cyclic behaviors

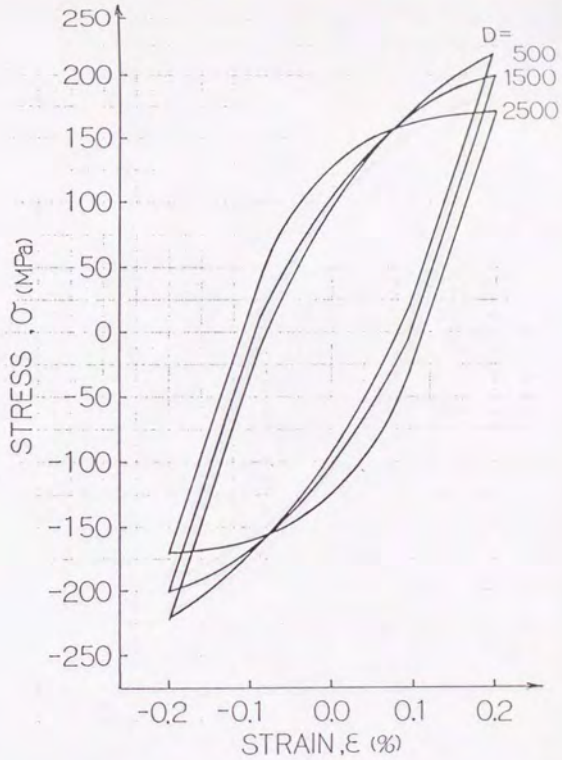

Figure 3.3.3.4 : Influence of the parameter D on the simulated cyclic behaviors

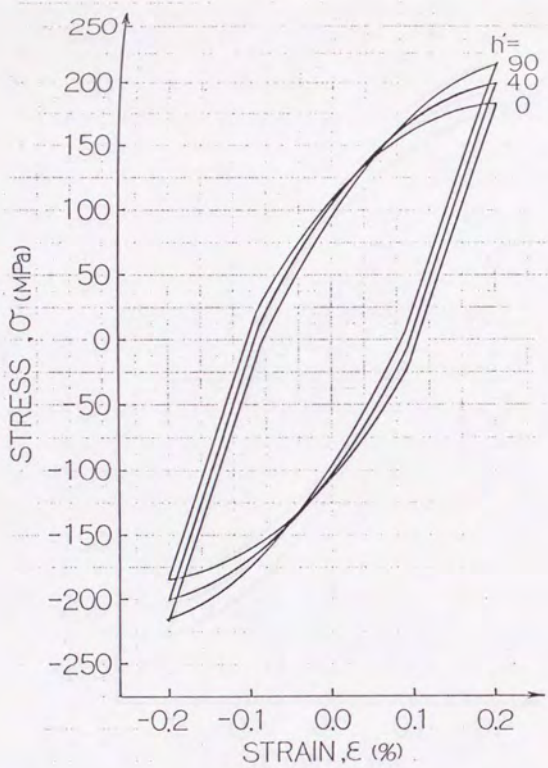

Figure 3.3.3.5 : Influence of the parameter h on the simulated cyclic behaviors (h' = h / d - k)

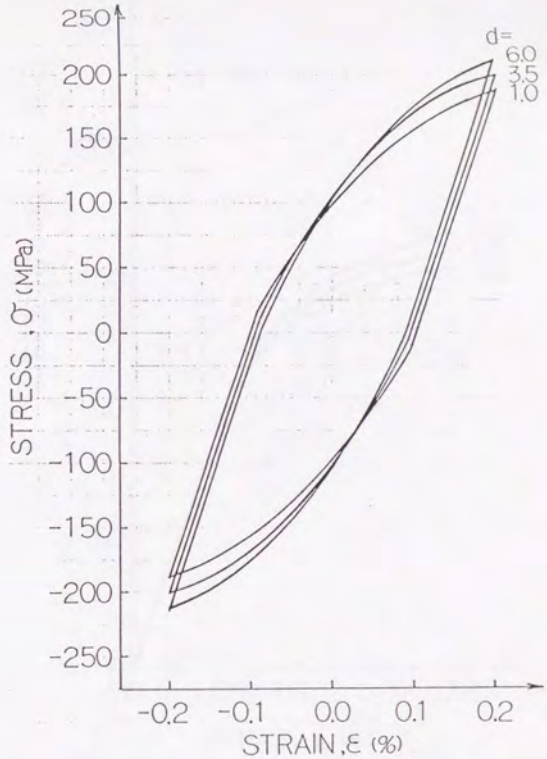

Figure 3.3.3.6 : Influence of the parameter d on the simulated cyclic behaviors

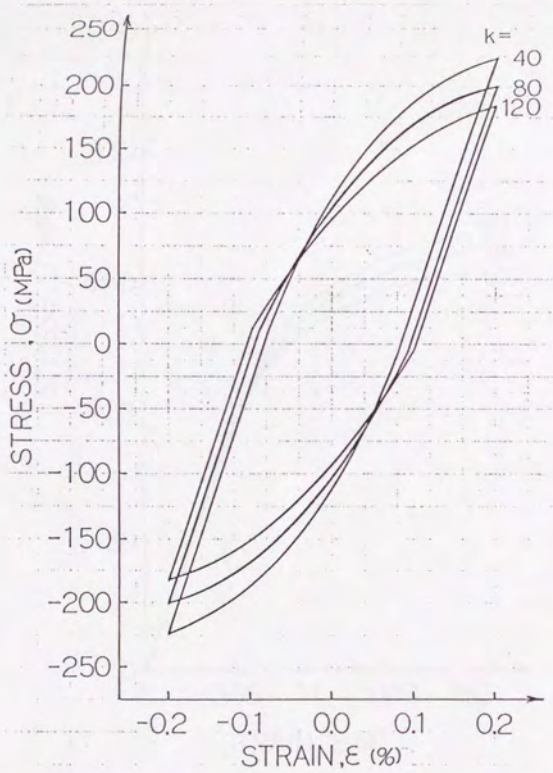

Figure 3.3.3.7 : Influence of the parameter k on the simulated cyclic behaviors

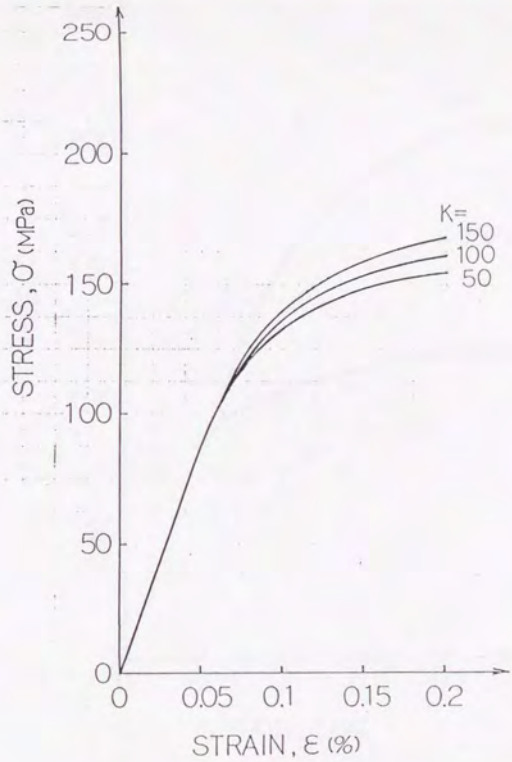

Figure 3.3.3.8 : Influence of the parameter K on the simulated tensile behaviors

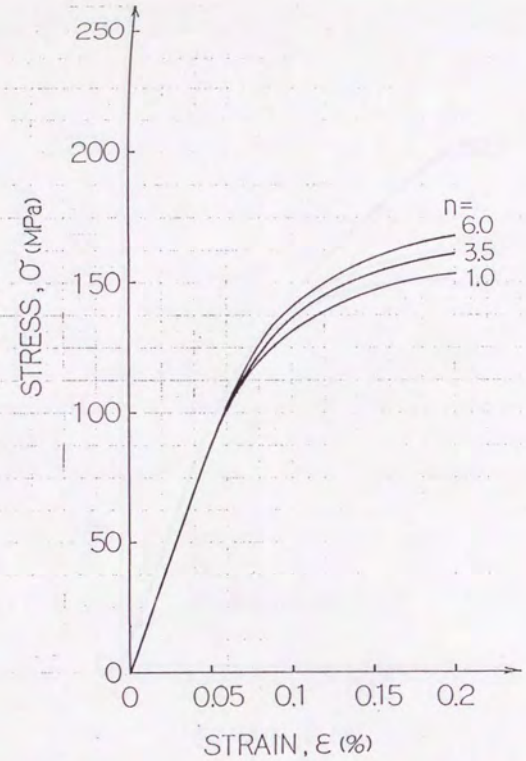

Figure 3.3.3.9 : Influence of the parameter n on the simulated tensile behaviors

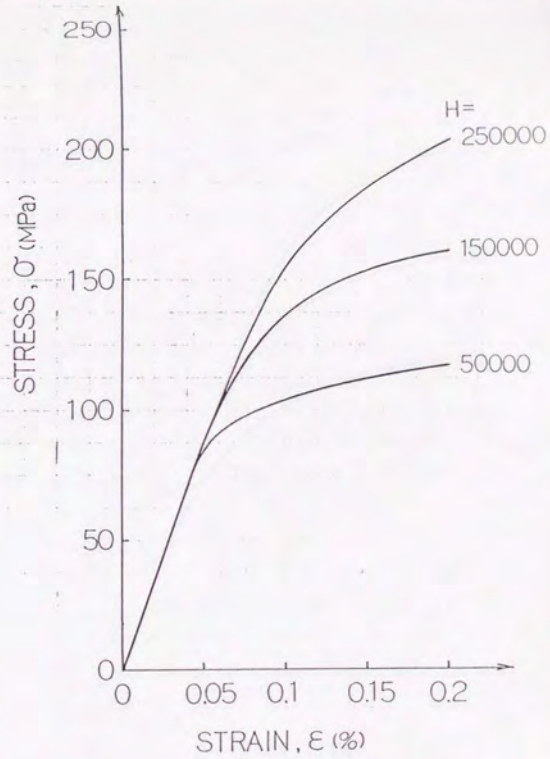

Figure 3.3.3.10 : Influence of the parameter H on the simulated tensile behaviors

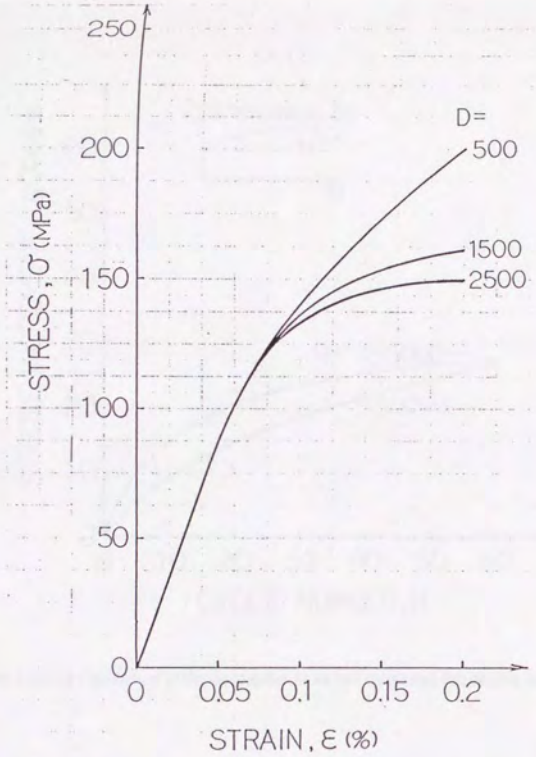

Figure 3.3.3.11 : Influence of the parameter D on the simulated tensile behaviors

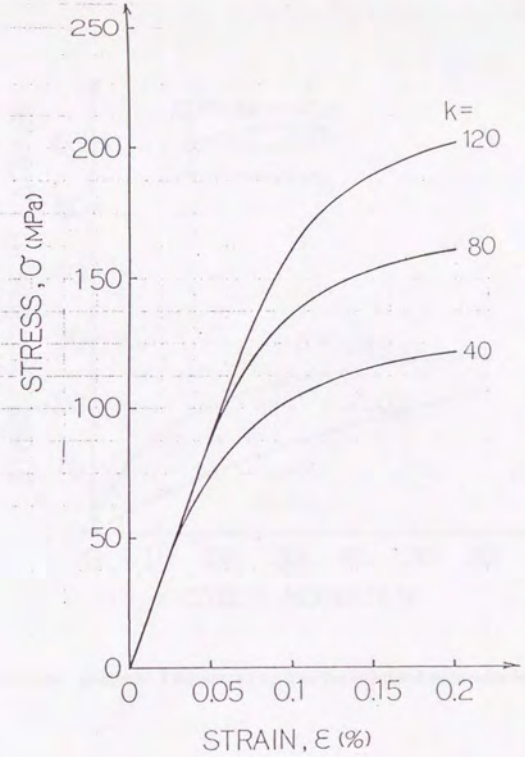

Figure 3.3.3.12 : Influence of the parameter k on the simulated tensile behaviors

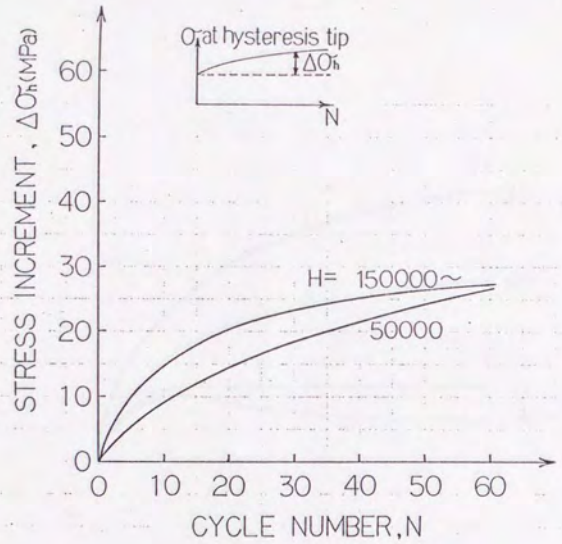

Figure 3.3.3.13 : Influence of the parameter H on the simulated hardening behaviors

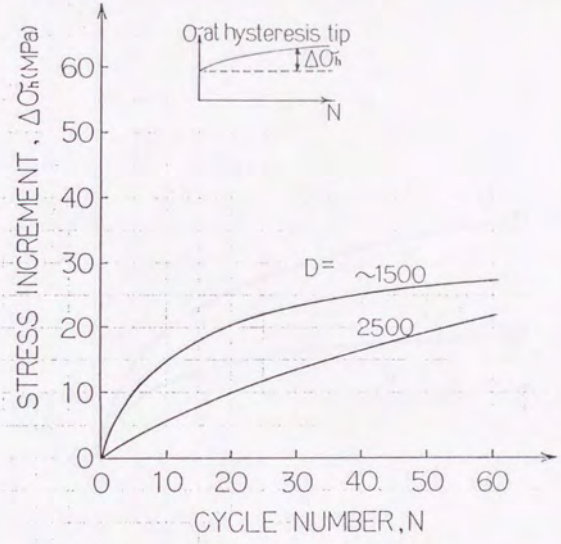

Figure 3.3.3.14 : Influence of the parameter D on the simulated hardening behaviors

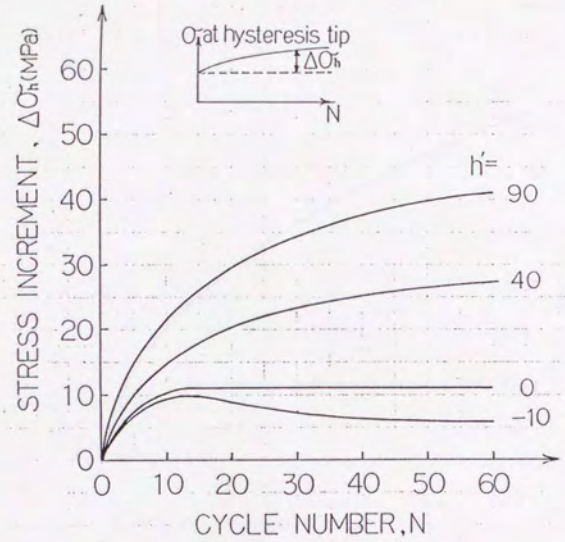

Figure 3.3.3.15 : Influence of the parameter h on the simulated hardening behaviors (h' = h / d -k)

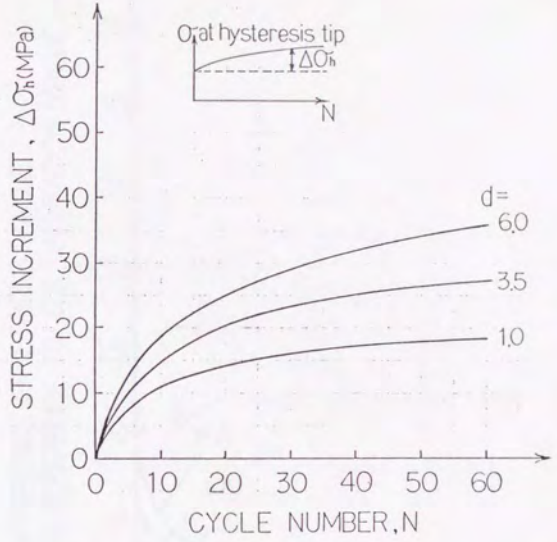

Figure 3.3.3.16 : Influence of the parameter d on the simulated hardening behaviors

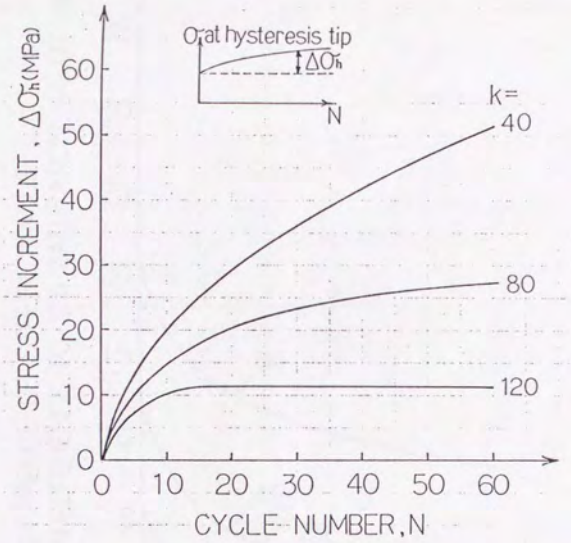

Figure 3.3.3.17 : Influence of the parameter k on the simulated hardening behaviors

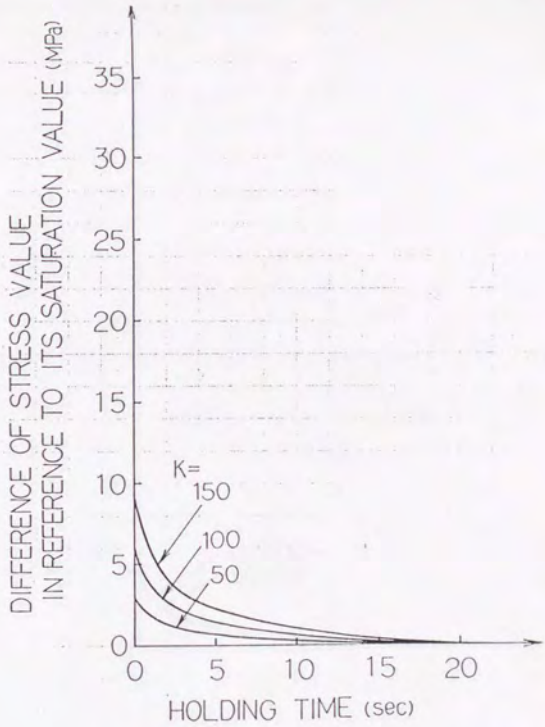

Figure 3.3.3.18 : Influence of the parameter K on the simulated relaxation behaviors

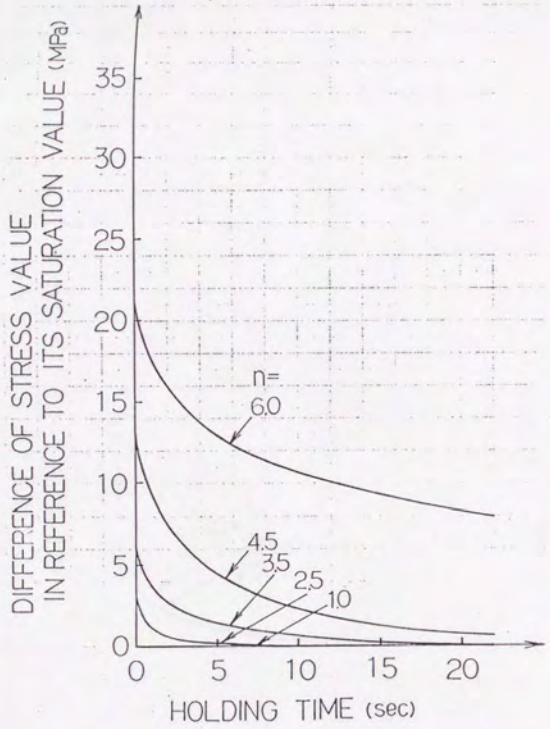

Figure 3.3.3.19 : Influence of the parameter n on the simulated relaxation behaviors

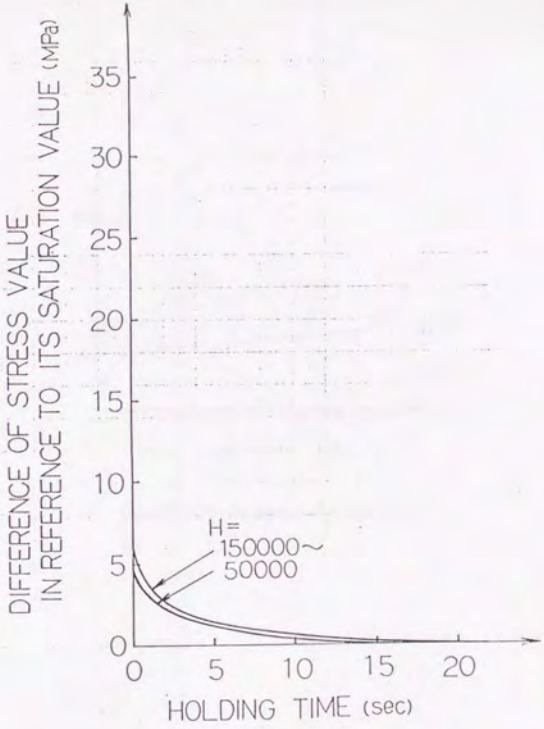

Figure 3.3.3.20 : Influence of the parameter H on the simulated relaxation behaviors

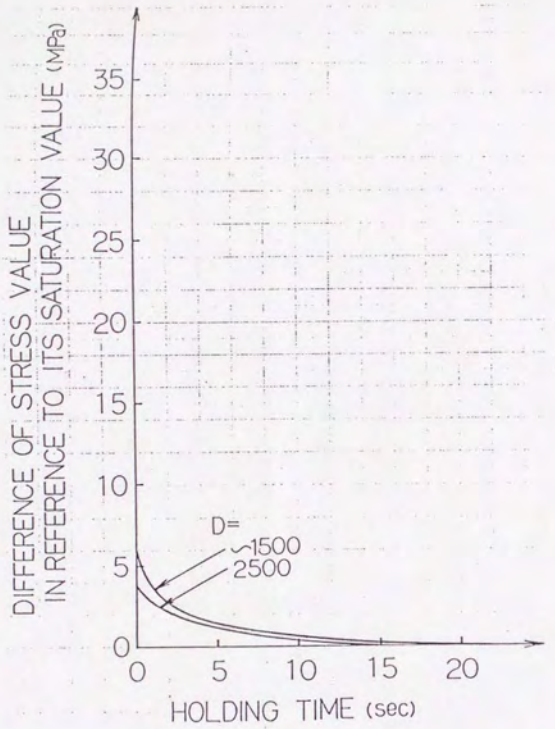

Figure 3.3.3.21 : Influence of the parameter D on the simulated relaxation behaviors

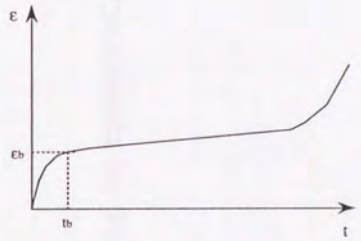

Figure 3.3.3.22 : An example of a creep curve

4 Experiments for Parameter Identification

4.1 Outline of Experiments

In order to evaluate Chaboche's parameters mentioned in the previous chapter, experimental data are necessary. While the methods to evaluate them are to be explained in the next two chapters, the procedures and the results of experiments are explained in this chapter.

Cyclic loading tests and succeeding relaxation tests were carried out under a stationary temperature and uniaxial stress condition. Furthermore, the beginning of each experiment (the simple tensile domain at the first quarter-cycle) was performed with monotonic loading starting at zero stress. From these experiments, the following data, which are required for the determination of parameters including confirmation of the characteristics of the evaluated parameter set, can be obtained :

1. stress-strain histories for the beginning tensile conditions (simple tensile curves),

2. stress-strain hysteresis loops under cyclic loading conditions (cyclic hysteresis curves),

3. stress histories at the hysteresis tips under cyclic loading conditions (cyclic strain hardening curves),

4. stress histories under relaxation conditions (relaxation curves).

A creep curve is normally taken into consideration especially to determine parameters K and n, but the above-mentioned set of reference curves with a relaxation curve can be regarded as sufficient.

The reasons why these experiments were employed to determine the parameters are as follows :

1. Some kinds of experimental tests are to be carried out in order to give the parameter set physical significance. The above-mentioned experiments are rather easier to be done from the point of obtaining accurate data than other kinds of tests, for example, primary creep tests.

2. Behaviors of back stress Y and yield stress R need cyclic loading tests to be separated.

3. Cyclic loading tests are interesting to be referred for the first wall condition due to cyclic operation of more than 10 cycles.

4. Cyclic loading tests are useful because a new numerical method to fit Chaboche's parameters to the hysteresis loops from cyclic loading tests has been developed in the present studies.

5. In cyclic loading tests, only small influence of inelastic strain rate $\dot{\varepsilon}^p$ to stress σ can be observed. That means, the effect of parameters K and n through the cyclic loading tests is not large enough to determine these parameters. On the other hand, relaxation tests show significant behaviors under these parameters. Hence, the experimental results from the relaxation tests can help to determine and to confirm parameter values of K and n.

With such simplified experimental conditions as the stationary and constant temperature condition, the uniaxial loading (stress) condition and the monotonic loading start at zero stress just at the beginning of each experiment, the simple form of Chaboche's viscoplastic theory is employed in the present studies. The Chaboche's parameters are found out one by one for the different temperature conditions. Therefore, sets of experiments were carried out under two different temperature cases of T=200℃ and T=400℃ (Ref. [4.1]). Here, for each temperature, several numbers of tests were performed to reduce the material behavior scattering to determine the parameters.

4.2 Test Specimens and Testing System

4.2.1 Configuration of the Test Specimens

The test specimen is not hour-glass shaped but has a cylindrical shape with the active length of 20mm and the diameter of 10mm at its central part. At the both edges, it has ribs for the attachment of axial displacement transducers also. Its configuration is drawn in Figure 4.2.1.1.

The hour-glass shaped specimen has been subject successfully to axially and diametrically controlled cyclic loading or fatigue test. Up to the total strain range of 1.5%, buckling dose not occur as described by Tjoa (Ref. [4.2]). In the present studies, the test specimen has a cylinder shaped part just only at its center in order to measure the displacement in the test specimen by a extensiometer. Since the hour-grass shaped test specimen was employed, correct measurement could be done due to the geometric change. On the other hand, if the tube shaped test specimen shown Figure 4.2.1.2 was employed to hold correctly the homogeneous and uniaxial condition, stress concentration might occur just near the border where the width of the test specimen

changes (at point A in Figure 4.2.1.2), which is not desirable for cyclic loading tests. The test specimen employed in the present studies can give the homogeneous and uniaxial condition at the tube shaped part and is suited to measure the strain correctly. The above mentioned advantageous characteristics of the hour-grass shaped test specimen can also be expected on the employed test specimen. The stress distributions on the surface of and in the test specimen are shown in Figure 4.2.1.3.

The test specimen which has been brought into the test is suited without irradiation.

4.2.2 Test Machine

A servohydraulic tension machine was used to carry out cyclic loading tests and relaxation tests (Ref.[4.3]). This machine can give the test specimen a certain load, displacement or strain condition controlled by electric circuits. The whole experimental system is shown in Figure 4.2.2.1.

In these studies, all experimental tests were carried out under strain controlled status. This machine is connected with a computer terminal through which such test conditions as strain rate, strain value (or expected stress value under stress controlled status) and hold time length can be controlled. A computer allows to give the planned stress and strain on a test specimen.

During the experiments, the jig and the test specimens can be completely covered with a furnace and their thermo-atmosphere is measured by means of thermo-couples to keep the test specimen under nearly constant temperature (error of less than 1℃) automatically. The thermal strain caused by the temperature rise before reaching the stationary thermo-atmosphere is released before each experiment.

Various stress-strain data obtained from the experiments were recorded numerically onto a floppy disk and graphically on recording paper. The recorded experimental data were the stress-strain histories during cyclic tests, the stress values at the hysteresis tips of all the cycles during the cyclic tests, the strain histories during the cyclic tests and the stress histories during the relaxation tests.

4.2.3 Deformation Measuring System

The elongation of the cylindrical part of the test specimen can be measured by means of an extensiometer (Ref. [4.4]). The structure of an extensiometer is shown in Figure 4.2.3.1. From one side, it grasps with two ceramic holding units inside the furnace at the polished surface of the test specimen. The attachment to the test specimen is shown in Figure 4.2.3.2.

The extensiometer gives an electrical voltage output in proportion to the elongation. The electrical

voltage output is measured and recorded digitally. After some measurements, it has been confirmed that this measuring system works very correctly within the error band of 1%.

4.3 Experimental Procedures

4.3.1 Experimental Conditions

Several sets of a cyclic test and a succeeding relaxation test were carried out under each temperature condition of T = 200℃ or 400℃. Figures 4.3.1.1 and 4.3.1.2 show typical loading histories, for examples, the former being for cyclic tests only with different strain conditions and the latter being for a cyclic and a succeeding relaxation tests.

The experiments are named as shown in Table 4.3.1.1. The cyclic loading tests were named as 'V01', 'V02'....,'V27'. Tests 'V01' to 'V06' did not lead to reliable results due to mechanical noises or system problems. Experiments V14 to V18 were carried out under the room temperature (T = about 20℃) as the reference data. Tests V08, V09, V11, V13, V19, V20 and V21 were carried out under the temperature condition of 200℃, and tests V07, V10, V12, V22, V23, V24, V25, V26 and V27 were carried out under the temperature condition of 400℃. On the other hand, the relaxation tests were named as 'R01', 'R02'...., 'R14'. Tests R01 to R05, R06 to R08 and R09 to R14 were carried out under the room temperature condition (T = about 20℃) as the reference data, under the temperature condition of 200℃ and under the temperature condition of 400℃, respectively.

4.3.2 Cyclic Loading Tests

Cyclic loading tests have been so designed as to give the test specimen a repeated load under a strain control operation. The type of the loading history is shown in Figure 4.3.2.1, where the total strain rate $\dot{\varepsilon}$, strain range $\Delta\varepsilon$ and strain amplitude are defined.

During the experiments, mean strain values, strain rates and strain ranges were continuously varied in the same cyclic test to obtain various experimental data under different conditions to give more detailed evaluation of the parameters. The strain ranges $\Delta\varepsilon$ and the strain rates $\dot{\varepsilon}$, for examples, were 0.3%, 0.4%, 0.6% and 0.8%, and 2.0×10^{-3} /sec, 2.0×10^{-4} /sec, 2.0×10^{-5} /sec and

2.0×10^{-6} /sec, at random respectively. The time table of strain conditions, strain range $\Delta\varepsilon$, strain rate $\dot{\varepsilon}$ and mean strain value ε_{mean} during each cyclic test V07 to V13 is shown in Tables 4.3.2.1 to 4.3.2.6. The first strain conditions of tests V14 to V27 are of the same strain ranges as those of tests R01 to R14 with strain rate of 2.0×10^{-4} /sec and mean strain value of 0.0%, respectively. Each cyclic test with the initial set of strain conditions was performed continuously over seventy cycles to reach the saturation.

4.3.3 Relaxation Tests

After such sufficient cycles of loading, isotropic hardening can be expected to be saturated. The holding time in relaxation tests was employed to be about a day, which is long enough for the saturation of over stress.

The holding strain value of every relaxation test was the same as the value at the end of the previous cyclic test as shown in Table 4.3.3.1. In all the relaxation tests, the total strain rate $\dot{\varepsilon}$ is theoretically zero, and the inelastic strain rate $\dot{\varepsilon}^p$ can be calculated as follows :

$$\dot{\varepsilon}^p = \dot{\varepsilon} - \dot{\varepsilon}^e = -\dot{\varepsilon}^e = -\frac{1}{E}\dot{\sigma} \qquad (4.3.3.1)$$

4.4 Experimental Results

4.4.1 Material Behaviors from Cyclic Tests

The cyclic curves were obtained from the cyclic loading experiments. The strain rate dependency after the first saturation (the saturation during the sufficient cycles of the first cyclic domain before changing the strain conditions) can not be found appreciably.

4.4.2 Behaviors from Relaxation Tests

The relaxation curves were obtained from the relaxation experiments. No appreciable stress relaxation can be found, which suggests that the employed material type SS 316L SPH stainless steel shows no considerable viscoplasticity.

4.4.3 Evaluation of Young's Modulus

Since the Young's modulus E of type SS 316L SPH stainless steel is needed to the presently proposed parameter identification procedures (both a numerical one and a neural one), it should be determined in this section. Its value is dependent on the temperature condition, and the values for both temperature cases of T = 200℃ and 400℃ should be determined based on the experimental hysteresis curves.

At first, the Young's modulus corresponding to each cyclic test was calculated graphically, where the steepness of the line slop ($\Delta\sigma/\Delta\varepsilon$) corresponds to the Young's modulus. The cyclic dependency and the material scattering of the Young's modulus value were discussed, while no cyclic dependency should exist in the material-model. Then, the average value of the Young's modulus for each temperature case was decided to be the value employed in the parameter identifications.

Step 1 : On the graphic paper, the best line which is starting at the zero point ($(\sigma, \varepsilon) = (0, 0)$) was fitted manually to the experimental curve from each test. The fitting was done to the first quarter cycle (the first tensile domain), the first cycle and the latter cycle, about the sixtieth cycle, in order to consider the cyclic dependency of the Young's modulus value. The results are shown in Table 4.4.3.1, where 'B', 'F' and 'L' mean the beginning quarter cycle, the first cycle and the latter cycle, respectively.

Step 2 : Next, comparing the evaluated cycle-dependent Young's modulus values, some difference between the values for 'B' and 'F' could be recognized, for example, about 20% difference for V13, while no appreciable cycle dependency could be found between those for 'F' and 'L'. Actually, no appreciable cyclic dependency after the thirtieth cycle to the saturation was observed. At the beginning of the experiment, the test specimen set up conditions could be different for each experiment. If the test specimen was set up with a little bend, the measurement by means of an extensiometer before the first cyclic tip should normally show a wrong tensile behavior, while such phenomena were observed actually. Therefore, the Young's modulus for all the cycles except for the first quarter cycle may be available. In the present studies, the average of the evaluated values for the first cycle and the latter cycle may be regarded as the accurate Young's modulus values. Table 4.4.3.2 shows the average value for each available experiment.

Step 3 : Finally, the average values of the Young's modulus were obtained from each experiment

for both temperature conditions, which reduce the data scattering. Table 4.4.3.3 shows the final evaluation results of Young's modulus for the both temperature cases of T = 200℃ and 400℃. The data scattering is larger under the higher temperature condition than under the lower temperature condition.

By the way, other numerical or systematic methods to evaluate the Young's modulus may be found. However, the experimental curve shows no clear bending in its configuration just near the border between the elastic and the inelastic domains. Therefore, it is difficult to evaluate the Young's modulus value with detailed reference to the experimental data (see Appendix 2), and the manual method employed in this section can be regarded as one of the best way to evaluate the Young's modulus value .

Table 4.3.1.1 : Names of the performed experiments and the temperature atmosphere

name of cyclic test	name of relaxation test	temperature atmospher (℃)
V01	-	-
V02	-	-
V03	-	-
V04	-	-
V05	-	-
V06	-	-
V07	-	400
V08	-	200
V09	-	200
V10	-	400
V11	-	200
V12	-	400
V13	-	200
V14	R01	R.T (about 20)
V15	R02	R.T (about 20)
V16	R03	R.T (about 20)
V17	R04	R.T (about 20)
V18	R05	R.T (about 20)
V19	R06	200
V20	R07	200
V21	R08	200
V22	R09	400
V23	R10	400
V24	R11	400
V25	R12	400
V26	R13	400
V27	R14	400

Table 4.3.2.1 : Loading history for V07

term number	cycle number of the term	the last cycle of the term	strain range $\Delta\varepsilon$ (%)	strain rate $\dot{\varepsilon}$ (/sec)	mean strain value ε_{mean} (%)
1	48	48	0.4	2.0×10^{-4}	0.0

Table 4.3.2.2 : Loading history for V08

term number	cycle number of the term	the last cycle of the term	strain range $\Delta\varepsilon$ (%)	strain rate $\dot{\varepsilon}$ (/sec)	mean strain value ε_{mean} (%)
1	48	48	0.4	2.0×10^{-4}	0.0

Table 4.3.2.3 : Loading histories for V09 and V10

term number	cycle number of the term	the last cycle of the term	strain range $\Delta\varepsilon$ (%)	strain rate $\dot{\varepsilon}$ (/sec)	mean strain value ε_{mean} (%)
1	60	60	0.4	2.0×10^{-4}	0.0
2	20	80	0.4	2.0×10^{-3}	0.0
3	2	82	0.4	2.0×10^{-6}	0.0
4	15	97	0.4	2.0×10^{-5}	0.0
5	15	112	0.4	2.0×10^{-4}	0.0
6	8	120	0.4	2.0×10^{-5}	0.0
7	20	140	0.4	2.0×10^{-3}	0.0
8	20	160	0.6	2.0×10^{-4}	0.0

after the 9th term, mean strain value were sifted at random.

Table 4.3.2.4 : Loading history for V11

term number	cycle number of the term	the last cycle of the term	strain range $\Delta\varepsilon$ (%)	strain rate $\dot{\varepsilon}$ (/sec)	mean strain value ε_{mean} (%)
1	71	71	0.4	2.0×10^{-4}	0.0
2	14	85	0.4	2.0×10^{-6}	0.0
3	15	100	0.4	2.0×10^{-4}	0.0
4	21	121	0.4	2.0×10^{-3}	0.0
5	10	131	0.4	2.0×10^{-5}	0.0
6	27	158	0.4	2.0×10^{-3}	0.0
7	3	161	0.4	2.0×10^{-6}	0.0
8	20	181	0.4	2.0×10^{-4}	0.0
9	20	201	0.6	2.0×10^{-4}	0.0

after the 9th term, mean strain value was sifted at random.

Table 4.3.2.5 : Loading history for V12

term number	cycle number of the term	the last cycle of the term	strain range $\Delta\varepsilon$ (%)	strain rate $\dot{\varepsilon}$ (/sec)	mean strain value ε_{mean} (%)
1	74	74	0.6	2.0×10^{-4}	0.0
2	11	85	0.4	2.0×10^{-6}	0.0
3	15	100	0.4	2.0×10^{-4}	0.0
4	21	121	0.4	2.0×10^{-3}	0.0
5	10	131	0.4	2.0×10^{-5}	0.0
6	27	158	0.4	2.0×10^{-3}	0.0
7	3	161	0.4	2.0×10^{-6}	0.0
8	20	181	0.4	2.0×10^{-4}	0.0
9	20	201	0.6	2.0×10^{-4}	0.0

after the 9th term, mean strain value was sifted at random.

Table 4.3.2.6 : Loading history for V13

term number	cycle number of the term	the last cycle of the term	strain range $\Delta\varepsilon$ (%)	strain rate $\dot{\varepsilon}$ (/sec)	mean strain value ε_{mean} (%)
1	61	61	0.6	2.0×10^{-4}	0.0
2	20	81	0.4	2.0×10^{-3}	0.0
3	2	83	0.4	2.0×10^{-6}	0.0
4	15	98	0.4	2.0×10^{-5}	0.0
5	15	113	0.4	2.0×10^{-4}	0.0
6	8	121	0.4	2.0×10^{-5}	0.0

after the 9th term, mean strain value was sifted at random.

Table 4.3.3.1 : Conditions of relaxation tests

$\Delta\varepsilon$	0.3%	0.4%	0.6%	0.8%
R.T	R01	R02, R03	R04	R05
T = 200℃	R06	R07	-	R08
T = 400℃	R09	R10, R11	R12	R13, R14

Table 4.4.3.1 : Evaluated Young's modulus for each cyclic test

test No.	temperature T (℃)	evaluated Young's modulus value (MPa)		
		B	F	L
V07	400	166531	172718	171467
V08	200	185993	186844	183962
V09	200	186595	188602	188602
V10	400	172550	173052	173052
V11	200	185592	184790	180863
V12	400	170945	168872	168872
V13	200	153088	183519	182181

Table 4.4.3.2 : Young's modulus corresponding to each cyclic test

test No.	average of F and L values (MPa)
V07	(172718 + 171467) / 2 = 172093
V08	(186844 + 183962) / 2 = 185403
V09	(188602 + 188602) / 2 = 188602
V10	(173052 + 173052) / 2 = 173052
V11	(184790 + 180863) / 2 = 182827
V12	(168872 + 168872) / 2 - 168872
V13	(183519 + 182181) / 2 = 182850

Table 4.4.3.3 : Young's modulus corresponding to each temperature

temperature T (℃)	average of F and L values (MPa)
400	(185403 + 188602 + 182827 + 182850) / 4 = 184921
200	(172093 + 173052 + 168872) / 3 = 171339

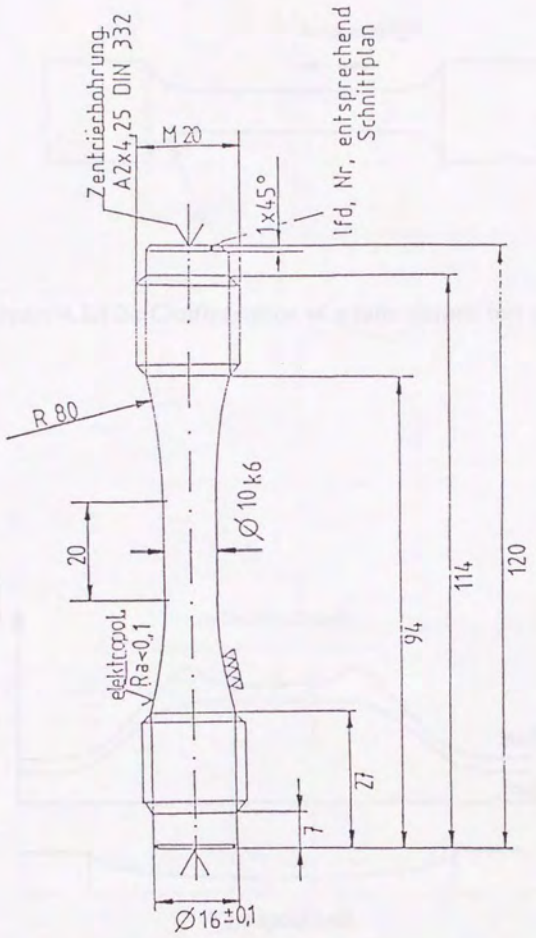

Figure 4.2.1.1 : Configuration of the test specimen

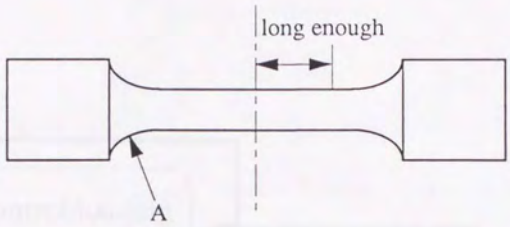

Figure 4.2.1.2 : Configuration of a tube shaped test specimen

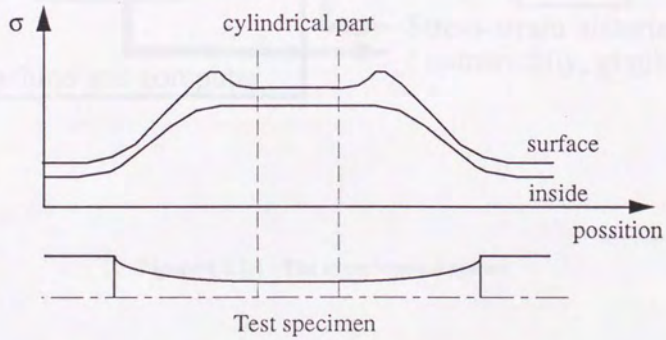

Figure 4.2.1.3 : Stress distributions on the employed test specimen

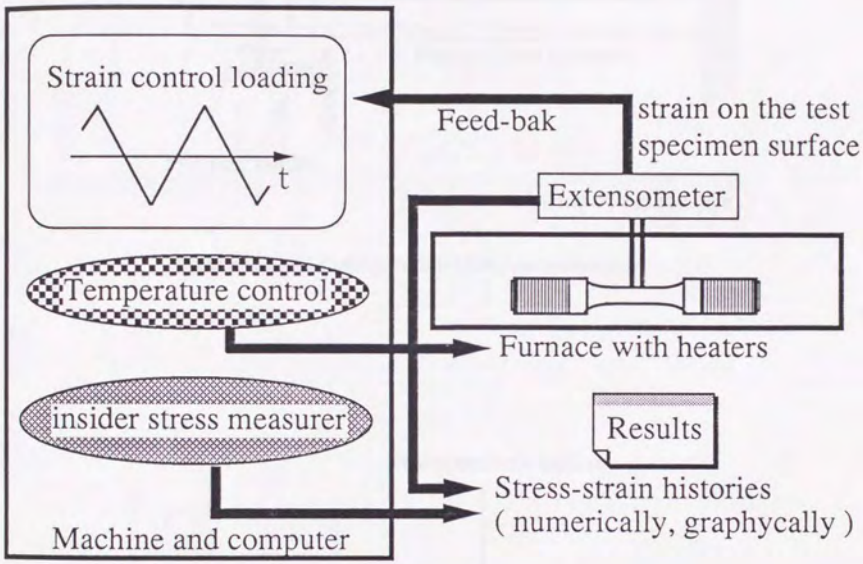

Figure 4.2.2.1 : The experimental system

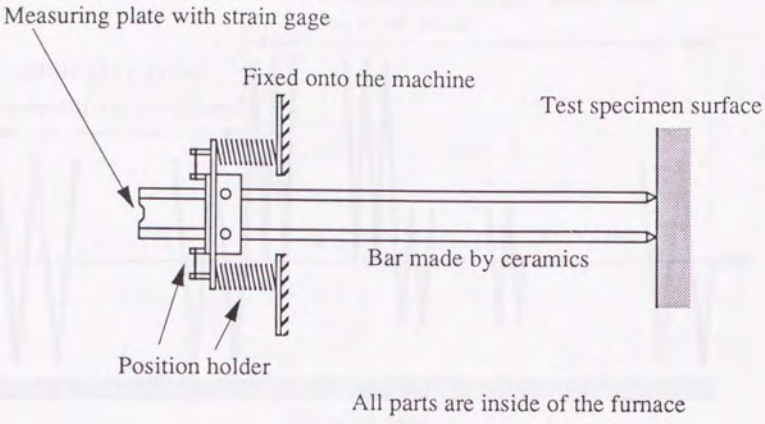

Figure 4.2.3.1 : Configuration of the extensiometer

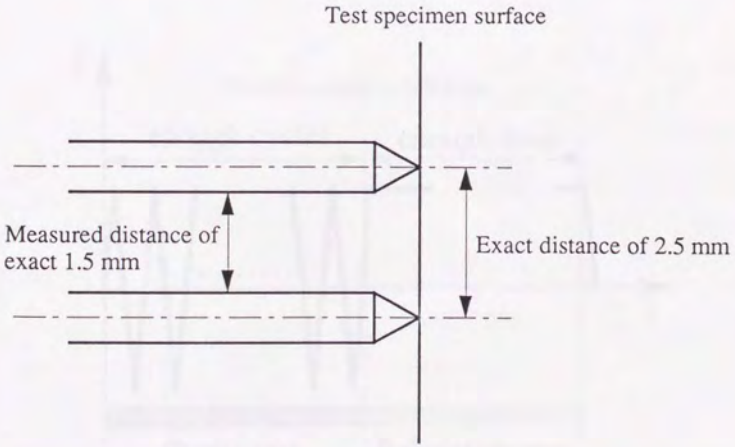

Figure 4.2.3.2 : Details of the attachment of the extensiometer to the test specimen

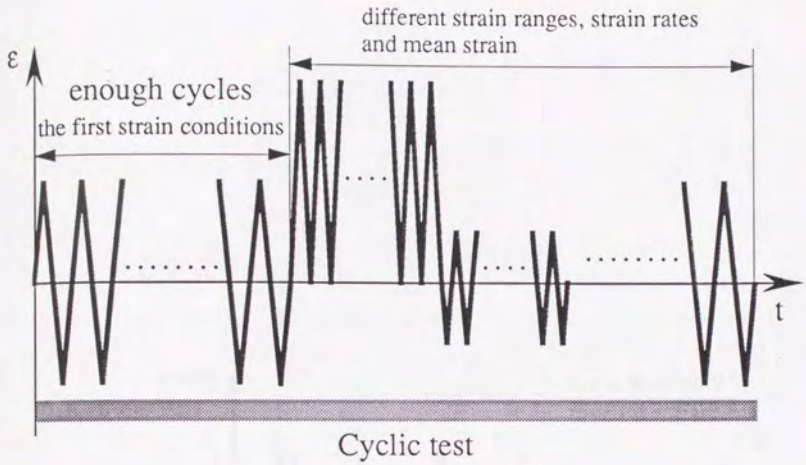

Figure 4.3.1.1 : Experimental loading history without a relaxation test

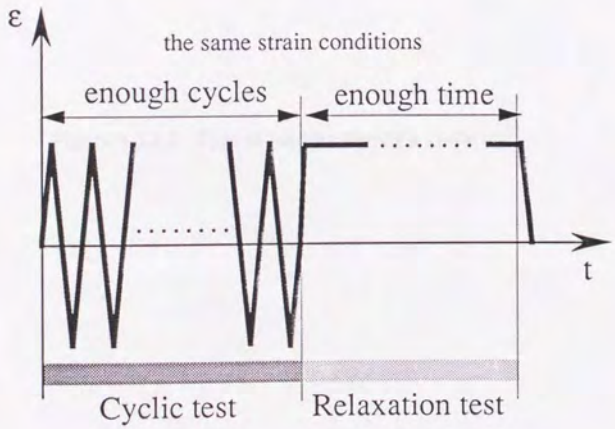

Figure 4.3.1.2 : Experimental loading history with a relaxation test

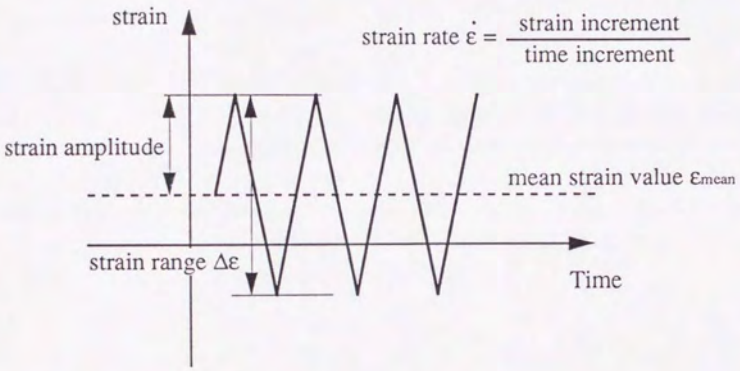

Figure 4.3.2.1 : Type of loading during a cyclic test